

SHEAR WAVE VIBRATIONAL DIRECTIONS AND
RELATED FAULT MOVEMENTS
IN SOUTHERN CALIFORNIA EARTHQUAKES

Thesis by
Peter Dehlinger

MAJOR THESIS
In Partial Fulfillment of the Requirements
for the Degree of
Doctor of Philosophy

California Institute of Technology
Pasadena, California

1950

ABSTRACT

Vibrational directions of direct shear waves from a number of small local earthquakes in southern California, recorded at Pasadena and Riverside, are determined and discussed in relation to corresponding faulting at the source. A theoretical relationship between small fault displacements and wave vibrational directions is proposed. Using this relationship, directions of SV and SH motions from various fault types at normal depths of focus are adduced. Observed initial shear wave motions indicate generally consistent SH, but usually less consistent SV displacements. Values SV/SH are consistent in a few localities, but generally vary widely. Polarization of SH waves is evidenced from the data; that of the SV is suggested, but is not so clearly indicated. Probably the entire shear wave is approximately plane polarized. From the data it appears that horizontal components of faulting in southern California, within local regions, usually take place in the same general direction. Vertical fault directions appear to vary. An analysis of faulting at the source, based on a comparison of observed SV and SH motions with theoretical shear motions and with observations by Gutenberg (1941) of impulses of compressional waves, is described. A fault pattern in agreement with the seismic data and also the regional surface geology involves primarily northwesterly trending right handed transcurrent faults in some parts of southern California, east west trending reverse or thrust faults in others, and coexistence of the two in a few localities. Somewhat simplified stress distributions in agreement with the data are discussed briefly. A method for determining strains of incident shear waves from linear strain seismograms, recorded through a new Benioff transducer and short period galvanometer, is also presented.

TABLE OF CONTENTS

	Page
Introduction	1
Acknowledgments	2
Theory	3
Method and Materials	20
Factors Affecting Reliability of Results	26
Distributions of Observed SV and SH Motions	31
Fault Patterns in Southern California	48
Possible Stress Distributions in Southern California	51
Appendix	55
References	63
Basic Data	66

INTRODUCTION

It is well known that first impulses of longitudinal waves depend on directions of fault displacements at the focus of an earthquake. Early literature on this subject has been summarized by Kawasumi (1937). Several Japanese writers, notably Honda (1932), Kawasumi (1933, 1934), Kawasumi and Yosiyama (1935), and Sezawa and Kanai (1936), have presented detailed mathematical treatments of vibrational properties of seismic waves. They have applied some of their analyses to specific Japanese shocks. Gutenberg (1941) investigated first impulses of longitudinal waves from a large number of southern California shocks, and discussed related fault motions. The purpose of the present investigation is to determine directions of initial motions of transverse waves from southern California shocks, and, if possible, correlate them with fault displacements.

Data for this study consist of initial amplitude measurements of shear waves recorded from more than 200 small local earthquakes occurring between 1941 and 1949. Only "direct" waves between the focus and surface were investigated in order to minimize effects of reflections and refractions on vibrational directions.

ACKNOWLEDGMENTS

I wish to express my sincere appreciation to Dr. B. Gutenberg who suggested this problem and supervised the work. Dr. H. Benioff proposed many ideas and criticisms, particularly about instrumentation. Dr. C. F. Richter contributed valuable suggestions. Helpful discussions with Dr. J. P. Buwalda and Mr. J. M. Nordquist are gratefully acknowledged.

THEORY

Vibrational directions of transverse waves, perpendicular to any ray paths, have been discussed by Gutenberg (1929). The wave motions can be described in terms of components u , horizontal in the plane of propagation, v , horizontal perpendicular to that plane, and w , vertical. Customarily, transverse waves are broken into SV and SH components, where the SV vibrate in the plane of propagation, containing the directions u and w , and the SH horizontally in the direction v (Fig. 1).

Amplitudes of SV and SH waves arriving at the earth's surface can be described as functions of ground displacements. Knott (1899) and Zoeppritz (1907, published posthumously) developed equations for the calculations of partitions of energies and amplitudes at discontinuities in the ground. The equations are also applicable at the earth's surface. Wiechert (1907) presented convenient equations relating ground motions to incident wave displacements at the surface. Gutenberg (1944b) reproduced Wiechert's equations and also presented curves which show the partitioning of SV energy and ratios of ground to incident displacement at the surface as functions of incidence angles. Calculations for these curves were made by Gutenberg (Zoeppritz, Geiger, and Gutenberg, 1912; Geiger and Gutenberg, 1912; and Gutenberg, 1944b) and Jeffreys (1926). The curves indicate the following relevant properties of incident SV waves:

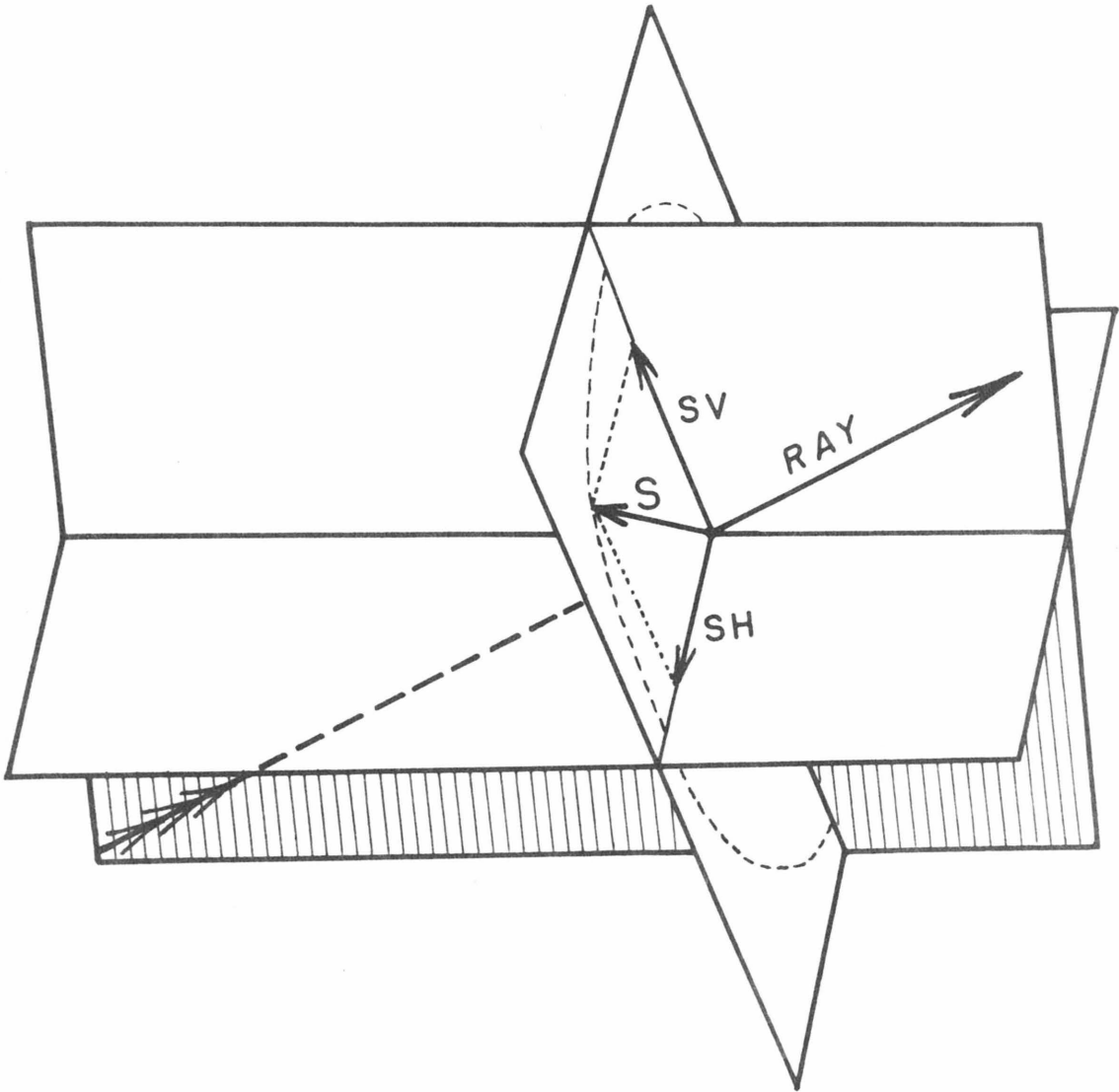


Fig. 1. Vibration directions of transverse waves. Planes shown are vertical, horizontal, and normal to the ray path.

At normal incidence, $i. = 0^\circ$, an SV wave is reflected at the surface as an SV with no change in phase; for the approximate range $0 < i. < 14^\circ$, an SV is reflected essentially as such with a minor part as a compressional (P) wave; for approximately $14^\circ < i. < 35^\circ$, most of the SV energy is reflected as P and a minor part as SV; for approximately $35^\circ < i. < 90^\circ$, an SV is reflected entirely as an SV, but involves a change in phase. For a Poisson's ratio of $\sigma = .239$, applicable in the "granitic" layer in southern California, it is seen that at $i. = 36^\circ$ an incident SV wave produces no vertical ground displacement; for the range $0 \leq i. < 36^\circ$, the vertical ground displacement is in the same direction as the corresponding component of the incident motion; for $36^\circ < i. < 90^\circ$, the vertical ground motion is in the opposite direction to the incident motion. Similarly, at $i. = 45^\circ$, an incident SV wave produces no horizontal ground displacement, u_3 , in the direction of propagation; for $0 \leq i. < 45^\circ$, u_3 is in the same direction as the corresponding component of incident motion; and for $45^\circ < i. < 90^\circ$, u_3 is in the opposite direction.

SH waves are reflected only as SH, regardless of incidence angle or value of Poisson's ratio; hence, incident SH amplitudes are half the magnitudes of the v_3 ground displacements (see also Bullen, 1947).

In the following, relationships between initial vibrational directions of transverse waves and corresponding fault motions are considered. Little is known about actual mechanisms of displacement during faulting, and only approximations can be simulated.

It is assumed that, during the time of faulting, energy is not transmitted across the fault plane in appreciable quantities as equal energies acting in opposite directions are released simultaneously from the two fault blocks. Some energy may be diffracted from one fault block into the other. Such energy will not only be comparatively small, but will be propagated somewhat later than the initial disturbance. It thus seems reasonable to expect initial compressional and shear waves to remain within the fault block in which they originate.

From observed ground displacements of large earthquakes, it would seem that small shocks of magnitudes 2.5 to 4.0 on the earthquake magnitude scale of Richter (1935) involve small displacements of probably less than a few feet. The length of faulting may be from several hundred meters to more than a km. At distances greater than several km from the source, waves generated from small faults will be nearly spherical in isotropic media. The wave fronts will consist of two separate sets lying on either side of a plane containing the fault surface. The displacement of a particle \bar{u} in such a wave front can be expressed by the known equation,

$$\frac{d^2 \bar{u}}{dt^2} = V_p^2 \text{grad div } \bar{u} - V_s^2 \text{curl curl } \bar{u} \quad (1)$$

where V_p and V_s are the compressional and shear wave velocities, respectively. The displacement \bar{u} can be represented by an irrotational component \bar{p} , where $\text{curl } \bar{p} = 0$, and a solenoidal component \bar{s} , where $\text{div } \bar{s} = 0$. Introducing $\bar{u} = \bar{p} + \bar{s}$ into the above equation leads to the familiar wave equations

$$\begin{aligned} \frac{d^2 \bar{p}}{dt^2} &= V_p^2 \nabla^2 \bar{p} \\ \frac{d^2 \bar{s}}{dt^2} &= V_s^2 \nabla^2 \bar{s} \end{aligned} \quad (2)$$

Expressions for displacement components of spherical waves in directions r, θ, φ , viz. p_r, p_θ, p_φ , and s_r, s_θ, s_φ , have been given by Kawasumi (1933) in terms of radial distances, Hankel cylindrical functions of the second kind, and surface harmonics of order n . Equations of these displacements indicate that compressional waves consist not only of a radial component, p_r , but also transverse components, p_θ and p_φ . The transverse components, however, are of higher order with respect to $1/r$ than the radial component. Similarly, shear waves consist of radial and transverse components s_r, s_θ , and s_φ , in which the radial component is of higher order with respect to $1/r$ than are the transverse. As spherical waves recede from the source, they approach true compressional and shear types of displacements.

If a small displacement acting over a small fault surface can be represented by equal and opposite vectors \bar{A} , then approximately spherical waves, formed within hemispheres in each fault block, would appear to have azimuthal symmetry about \bar{A} . Solutions of Kawasumi's equations implying azimuthal symmetry, and involving either one or two nodal cones in the wave fronts, indicate that the components of displacement p_r , p_θ , s_r , and s_θ exist, but that the components p_ϕ and s_ϕ vanish. A reasonable and physically intuitive assumption, which also results in azimuthal symmetry and not more than two nodal cones in the wave fronts, is that just beyond the zone of fracturing at the source a wave displacement \bar{u} is about parallel to a fault displacement \bar{A} . Since the components p_ϕ and s_ϕ are then nearly zero, displacements \bar{p} and \bar{s} will lie approximately in a plane formed by the vectors \bar{A} and \bar{R} , where \bar{R} is the ray path. Vectorially this relationship can be expressed as (Fig. 2)

$$\bar{A} \times \bar{R} \cdot \bar{s} \approx 0 \quad (3)$$

Based on equation (3), amplitudes of compressional and shear waves are related to the displacement \bar{u} by approximately (Fig. 2)

$$\begin{aligned} p &\approx u \cos \theta \\ s &\approx u \sin \theta \end{aligned} \quad (4)$$

Initial motions of shear waves resulting from fault displacements of small magnitudes can be approximated by equation (3). This is the analysis used in figures 3 through 8, in which surface

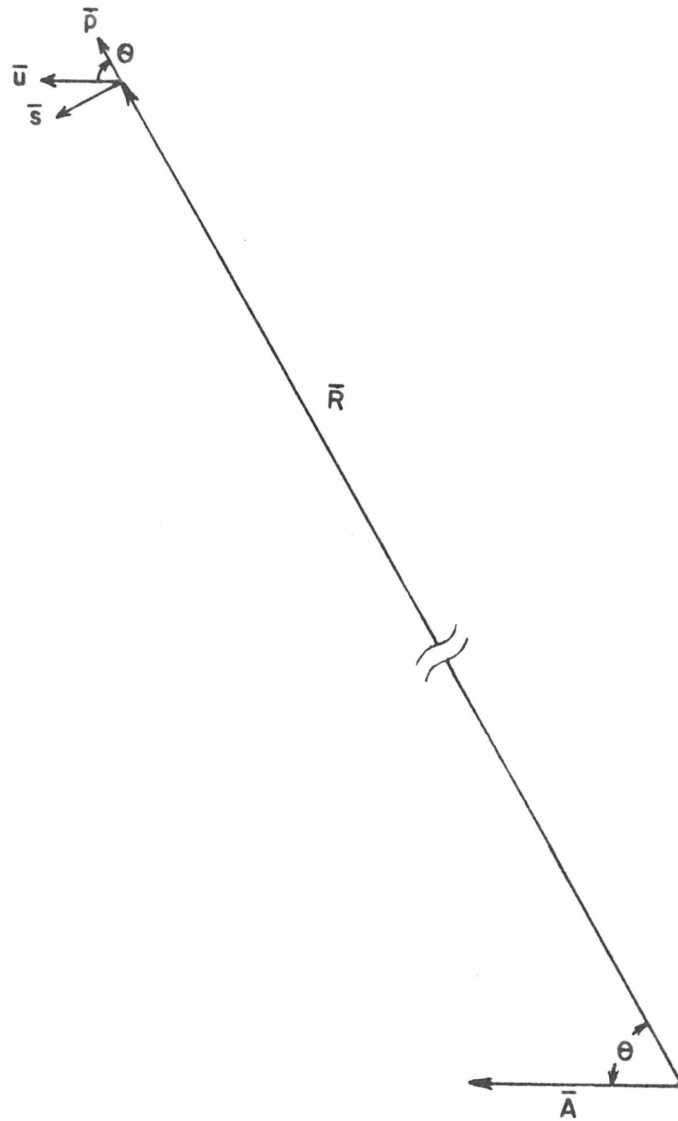


Fig. 2. Relationship between the direction of fault movement (\underline{A}), ray path (\underline{R}), and vibration directions \underline{p} and \underline{s} , assuming a displacement \underline{u} , just beyond the zone of fracturing, parallel to \underline{A} .

distributions of initial SV and SH displacements, generated from the following types of faults, are illustrated:

1. Transcurrent (strike slip)
2. Vertical, with vertical displacement
3. Horizontal
4. Normal
5. Reverse and thrust

Assumptions made in determining theoretical wave displacements in the discussion to follow are:

1. The earthquake originates at a point.
2. Fault displacements are linear.
3. Spherical waves are radiated (implying isotropic media).
4. Initial shear, and also compressional wave displacements remain in the same fault block in which they originate.

Transcurrent (strike slip) fault

Shear waves radiated horizontally from a transcurrent fault source consist of only SH components. Figure 3 illustrates distributions of initial SH motions for horizontal rays. Arrows in the plan view of the figure indicate directions of fault and wave motions. In the cross section, "in" refers to motion normal to and directed into the paper; conversely, "out" refers to motion out of the plane of the paper. From equation (4), it is seen that rays normal to the strike of the fault have the largest SH amplitudes for given radial distances; those in line with the fault have zero amplitudes. SH amplitudes are of intermediate magnitudes between these two directions.

Transcurrent faulting at normal depths of focus, about 16 km (Gutenberg, 1943, 1950) in southern California, produces the surface

distribution of motion illustrated in figure 4. In the plan view of the figure, arrows indicate initial motions in the horizontal directions u and v ; "up" and "down" indicate displacements in the vertical direction. At random wave path orientations, both SV and SH waves arrive at the surface. Only SH components exist in directions normal to the fault strike. Both SV and SH amplitudes are small in the vicinity of the plane containing the fault surface. The amplitude ratio SV/SH is usually less than unity in intermediate directions.

Vertical displacement (vertical fault)

Shear waves generated by vertical faults with vertical displacements consist of only SV components. SV amplitudes for the surface distribution illustrated in figure 5 are approximately constant at given radial distances, except near the plane containing the fault surface where they approach zero. Changing the focal depth for this type of fault alters the ratio u/w of the SV waves.

Horizontal fault

Horizontal faulting at normal depths of focus produces surface distributions of initial shear motions as shown in figure 6. Rays normal to the direction of faulting contain no SV components, those in the same direction no SH components. Generally, both SV and SH waves will arrive at the surface.

Normal fault

Normal faults having dips of approximately 60 degrees, and originating at about 16 km depths, produce initial SV and SH motions at the surface as illustrated in figure 7. Rays propagated perpendicular to the strike of the fault contain no SH components. In the vicinity of a plane containing the fault surface, SV and SH amplitudes are small and the ratio SV/SH is a minimum for the distribution shown on figure 7. SV and SH waves exist between these two directions and the ratio SV/SH is greater than unity for the fault dips assumed. The ratio increases as the dip of the fault increases.

Reverse and thrust faults

Dips of reverse and thrust faults, ranging from about 15 to 75 degrees and originating at normal depths of focus, result in identical surface distributions of initial SV and SH ^{directions of} displacements (Fig. 8). Rays perpendicular to the strike to the fault contain no SH components. In the vicinity of a plane containing the fault surface, SV and SH amplitudes are small and the ratio SV/SH is the smallest for the distribution shown on the figure. At random wave paths, both SV and SH waves arrive at the surface. The ratio SV/SH increases as the fault dip increases.

Each of the five fault types illustrated in figures 4 through 8, originating at normal depths of focus, is seen to result in distinctively different overall surface distributions of initial

SV and SH displacements. Accordingly, the figures seem to be diagnostic, for the given assumptions, in evaluating fault motions related to observed SV and SH displacements.

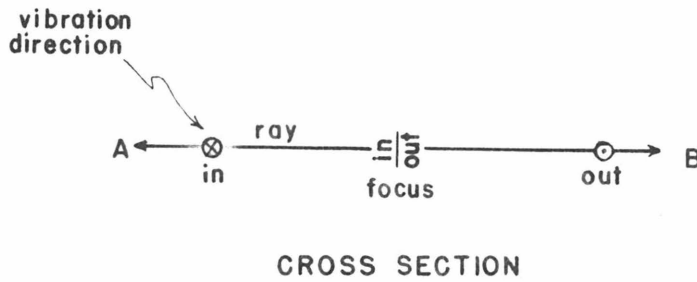
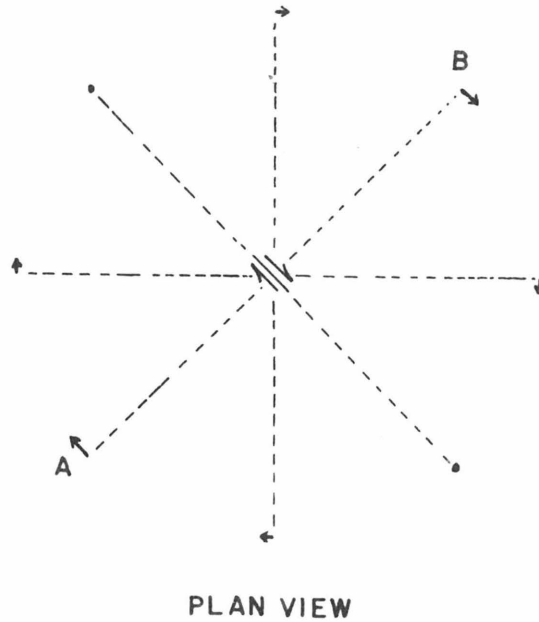


Fig. 3. Distributions of initial SH vibration directions radiated horizontally from a transcurrent fault. SV motions are zero for such wave paths. Motions in plane of paper indicated by arrows; motions perpendicular to paper indicated by "in" if directed into paper, and "out" if out of paper.

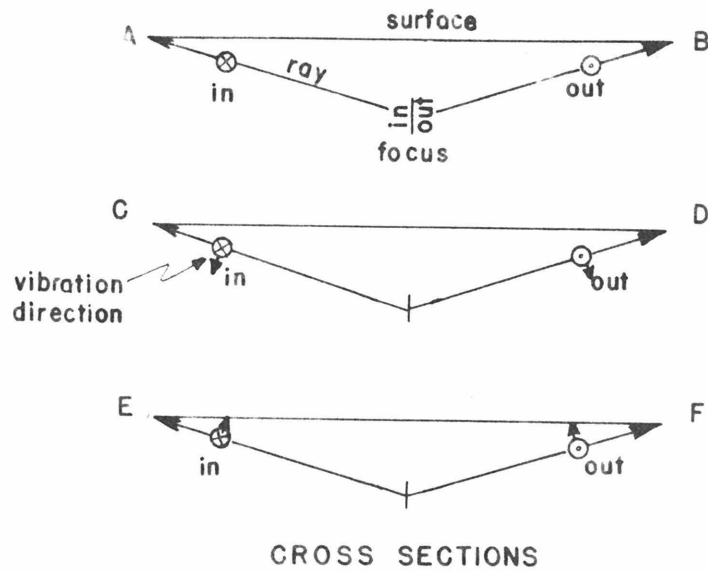
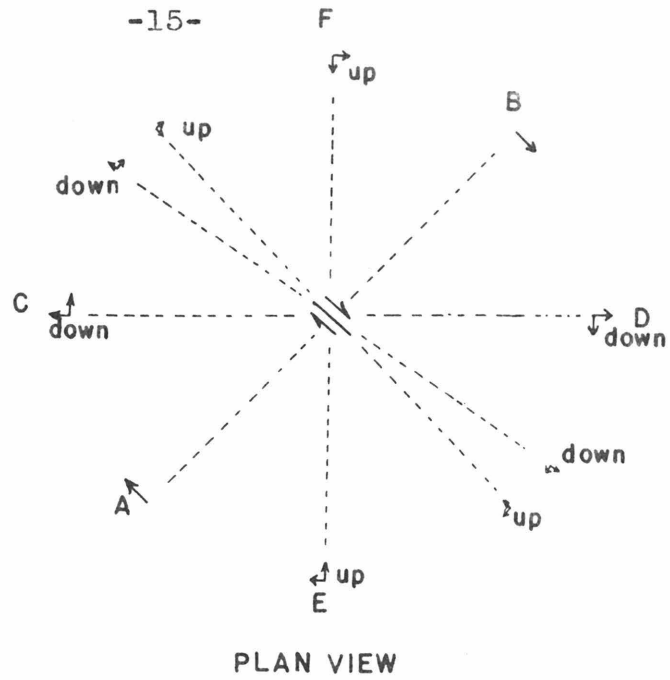


Fig. 4. Surface distributions of initial SV and SH motions generated by a transcurrent fault displacement at normal depth of focus. "Up" and "down" refer to directions of vertical components of SV.

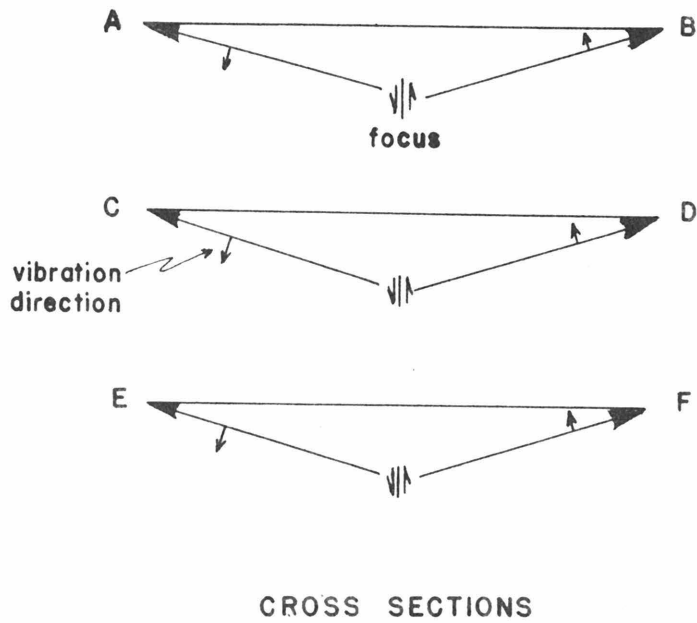
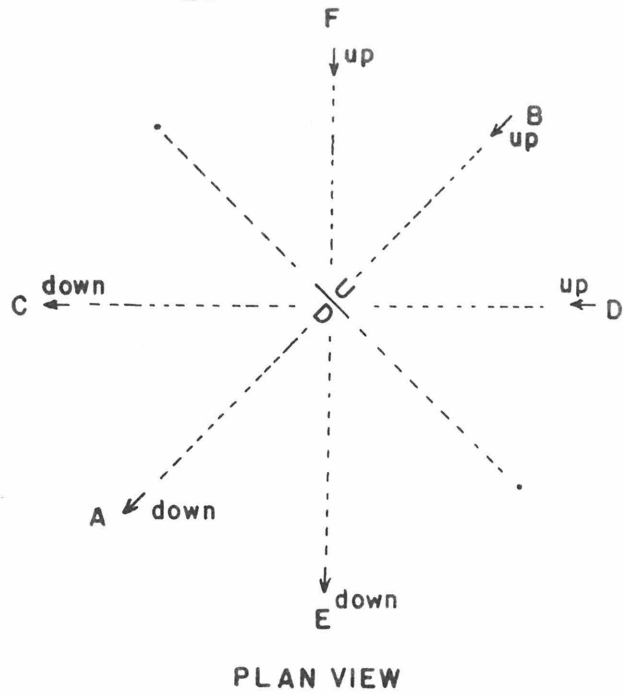
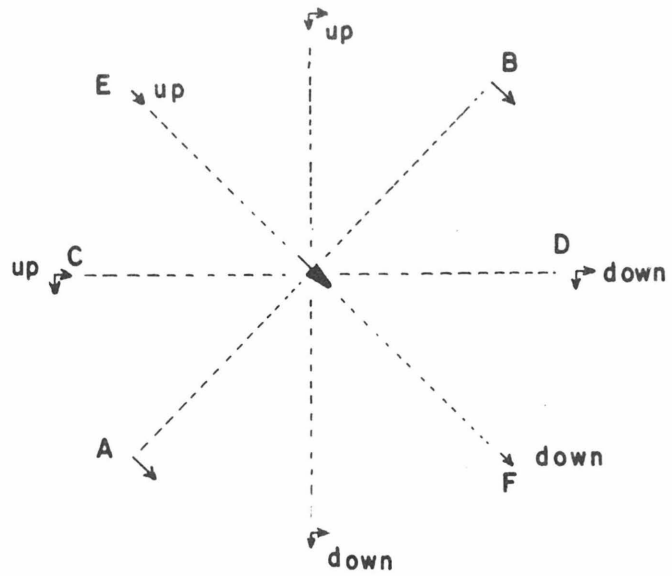
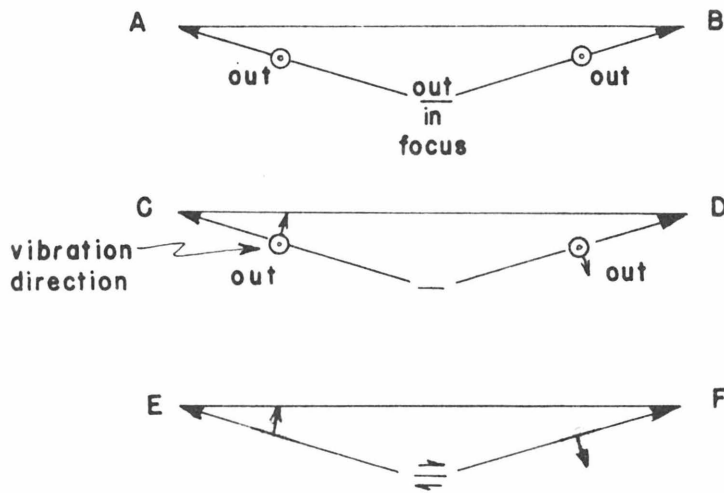


Fig. 5. Surface distributions of initial SV motions generated by a vertical fault displacement at normal depth of focus. No SH waves are generated by such fault movements.

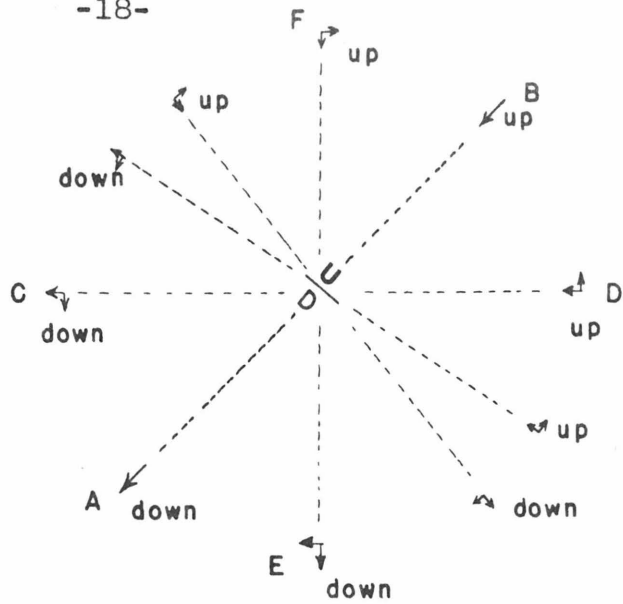


PLAN VIEW

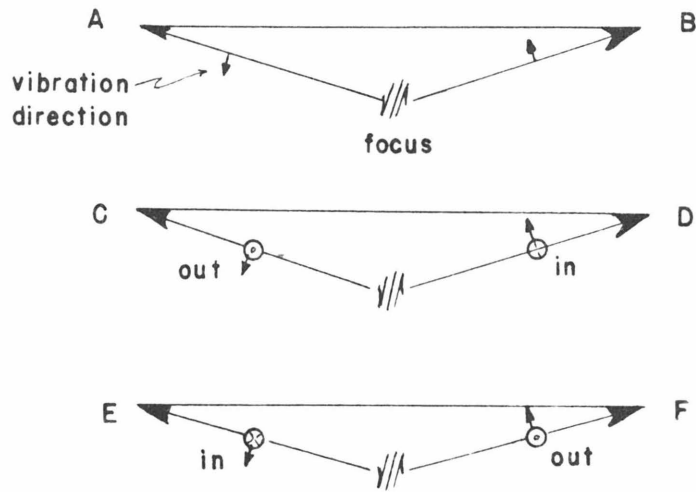


CROSS SECTIONS

Fig. 6. Surface distributions of initial SV and SH motions generated by a horizontal displacement at normal depth of focus.



PLAN VIEW



CROSS SECTIONS

Fig. 7. Surface distributions of initial SV and SH motions generated by a normal fault displacement at about a 16 km depth of focus.

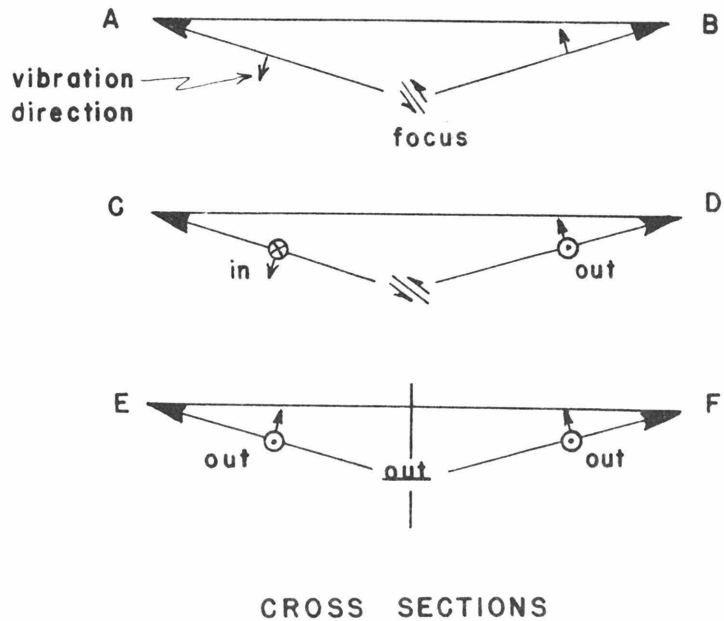
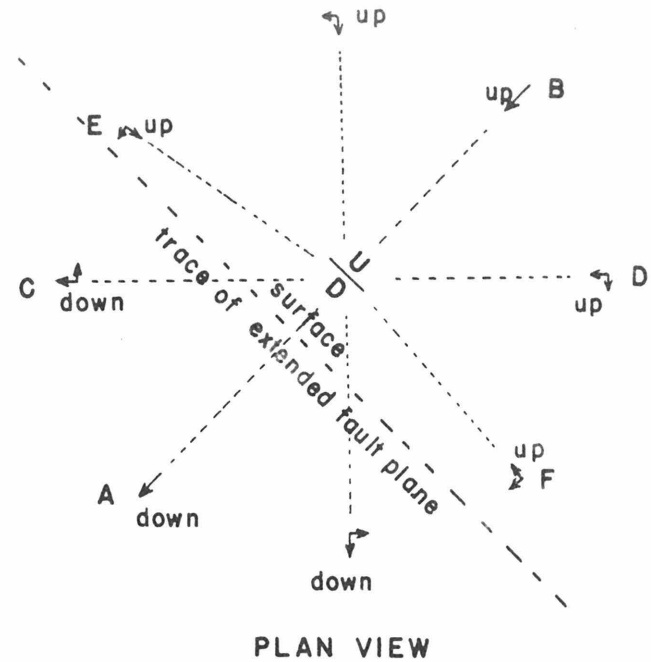


Fig. 8. Surface distributions of initial SV and SH motions generated by a reverse or thrust fault at normal depth of focus.

METHODS AND MATERIALS

In this study only "direct" transverse waves are used; this minimizes effects of reflections and refractions on original vibrational directions. The paths of these waves are assumed to be consistent with Gutenberg's (1950) recent hypothesis on the structure of the upper crust, in which horizontal layers of different velocities above the normal depth of focus are postulated (Fig. 9). The "direct" waves are consequently refracted to a minor extent within the upper crust. In southern California shocks, the direct transverse waves are the first shear waves to arrive at the surface for epicentral distances ranging from 0 to at least 130 km. For shocks beyond this epicentral range, waves refracted through deeper layers arrive before the "direct" wave.

Initial amplitudes of transverse waves from numerous local southern California earthquake records were measured in this study and resolved into corresponding incident motion. In the early stages of this research, begun prior to Dr. Gutenberg's layering hypothesis, amplitudes of \bar{S} , at that time considered to be the direct wave (see, e.g. Gutenberg, 1943, 1944a, 1945), were measured. Shocks ranging in epicentral distances from 0 to 75 km and 100 to 200 km were used. Those between 75 and 100 km were disregarded to avoid interference between \bar{S} and S_y energies. Under the new hypothesis, \bar{S} waves are the direct ones only for epicentral distances of less than about 75 km, and S_y for those of greater distances.

\bar{S} amplitude measurements for shocks at more than 100 km epicentral distances, accordingly, had to be discarded and were replaced by measurements of S_y waves for shocks between 75 and 130 km distances.

Small magnitude shocks, usually ranging from 2.5 to 4.0, with a few as large as 4.5 on the Richter (1935) earthquake magnitude scale, were used. Advantages in using small shocks are: (1) many records from random epicentral locations are available; (2) point source approximations at the focus, simplifying interpretations of the results, can be made.

Amplitude measurements were made on Pasadena and Riverside seismograms. Useful records from the Pasadena station were acquired from the following instruments.

- (1) Torsion seismographs; two horizontal components, natural period, 0.8 seconds; damping constant, 0.8.
- (2) Benioff electromagnetic seismographs; one vertical and two horizontal components; pendulum period 1 second; damping constant, 0.8; short and long period galvanometers, 0.2 and 90 seconds, respectively, recorded at each instrument.
- (3) Benioff strain seismographs; two horizontal components; instruments undamped; galvanometer period, 70 seconds.

Instruments at the Riverside station consist of two horizontal component torsion seismographs and one short period vertical

Benioff type. In this study records from only the horizontal seismographs are used. The Riverside instruments have nearly the same constants as the corresponding ones at Pasadena.

Short period torsion seismographs, recording through optical systems, provided the most useful records for this work. The magnification and response of these instruments to transient ground displacements are more reliably known than those of the Benioff type recording through electrical systems. Benioff instrument seismograms are used in this work primarily to check torsion record displacement directions.

Analyses of strains created by incident shear waves as recorded by Benioff strain instruments were attempted. The instruments are currently operating through 70 second galvanometers and do not approximate short period ground strains reliably. However, Benioff has recently developed a transducer which, on strain instruments recording through an 0.1 second galvanometer, will reproduce ground strains directly for all waves of periods greater than about 0.2 to 0.3 seconds. Strain instruments with such transducers and galvanometers may eventually be installed at the Palomar seismological station. In the appendix a procedure is given for determining incident shear wave strains with such strain seismographs.

Transverse waves were identified on the seismograms with the aid of southern California travel time curves (Gutenberg, 1944a). Initial amplitudes and corresponding periods of these waves were

measured. Magnification curves for instruments at the Pasadena station were used to obtain corresponding ground displacements. The same curves indicate ground displacements on the Riverside seismograms except for a constant "ground factor". Since amplitude ratios rather than absolute displacements are of interest in this study, the "ground factor" difference between the two stations is unimportant.

Periods recorded at Pasadena and Riverside ranged from 0.3 to 0.8 seconds. The torsion instruments at Riverside generally recorded slightly shorter periods than those at Pasadena.

Directions and magnitudes of total horizontal ground displacements were calculated as vector sums of north south and east west displacements. Horizontal components u in the direction of propagation and v normal to that direction were resolved from these total values. Vertical displacements w were obtained from vertical component instruments. In this study, u is defined positive when directed from the epicenter to station, v positive in a direction rotated 90 degrees clockwise from positive u , and w positive downward.

Incident SV and SH amplitudes were resolved from displacements u_g , v_g , and w_g in accordance with Wiechert's (1907) equations for partitions of amplitudes incident at the earth's surface. Incident SV amplitudes were determined from curves (Gutenberg, 1944b, fig. 3b, p. 99) relating amplitude ratios u_g/SV and w_g/SV to incidence angles i . With few exceptions SV amplitudes were obtained from u_g determinations as resolved from the torsion seismograms, although some

were obtained from w_g displacements based on electromagnetic instruments records. Incident SH amplitudes (see page 5) have comparatively simple reflection characteristics and are taken as half the magnitudes of the v_g ground displacements.

Incidence angles used for SV amplitude determinations are computed for direct rays, assuming a 16 km depth of focus and ray paths according to Gutenberg's (1950) crustal velocity distribution. Thicknesses and transverse velocities of the upper crustal layers are shown on figure 9. Incidence angles at both the source and the surface are also shown as functions of epicentral distances in this figure. In regions where there are no sedimentary rocks, the upper layer appears to be about 5 km thick and has a transverse velocity of 3.4 km/sec. A discontinuity is evidenced between this layer and that beneath it. This lower layer appears to have an average velocity of 3.8 km/sec. Its thickness is not known definitely but for computations of incidence angles, a reasonable value of 8 km is assumed. This zone grades into the one below it without evidence of discontinuity. In the vicinity of the 16 km depth the velocity has decreased to about $3\frac{1}{2}$ km/sec.

Initial SV and SH motions computed in this study are plotted on fault maps of southern California (figures 10 through 15). Observed displacements are plotted at the epicenters.

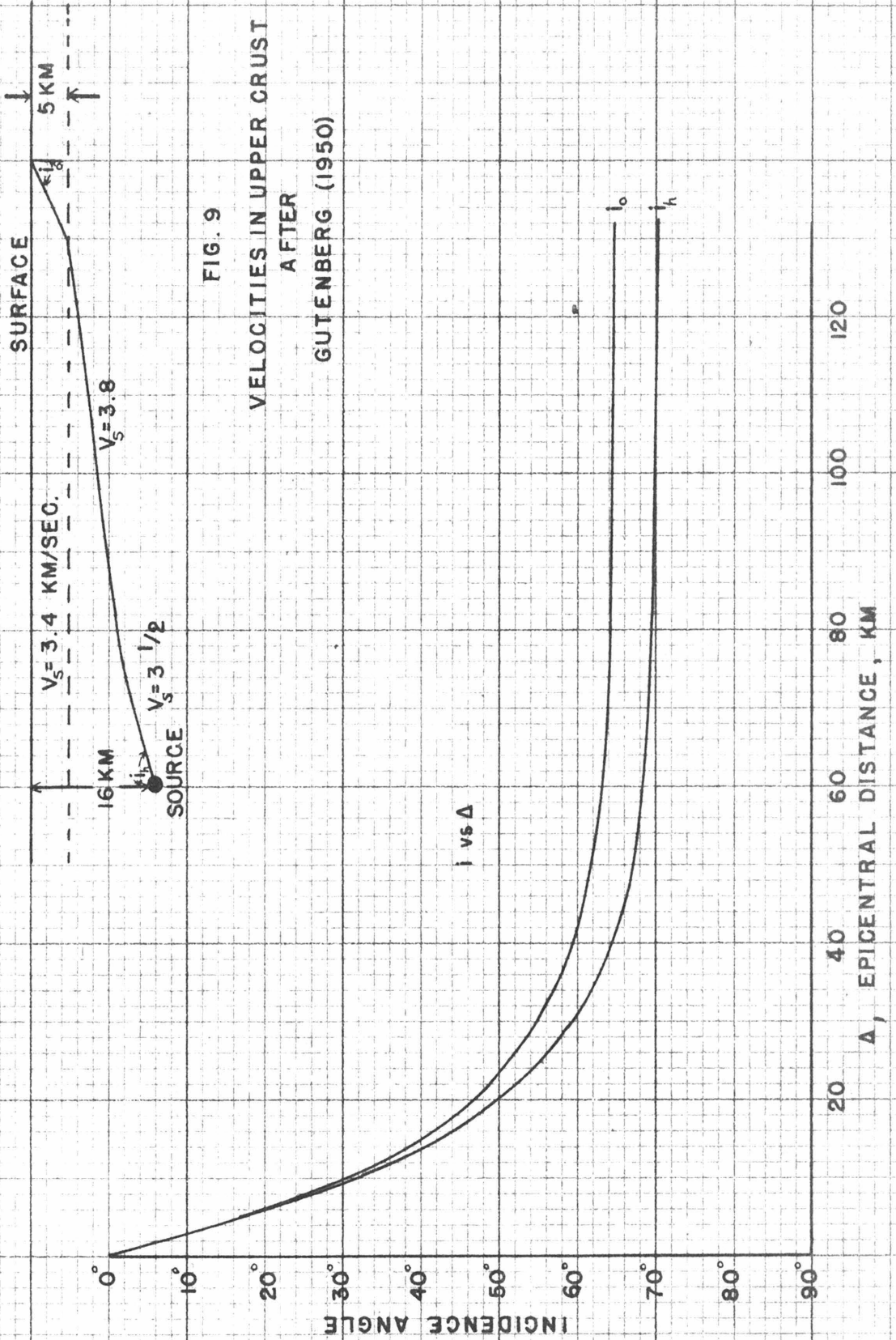


FIG. 9
VELOCITIES IN UPPER CRUST
AFTER
GUTENBERG (1950)

FACTORS AFFECTING RELIABILITY OF RESULTS

Factors affecting the reliability of resultant SV, SH, and SV/SH determinations are discussed in the following:

1. Reliability of assumed azimuths of rays

In this paper u is assumed to be directed from the epicenter to the station; v is assumed to be normal to this direction. Epicentral locations upon which these determinations depend are known within 5 to 15 km. Thus, except for shocks near the station, errors in epicentral locations will have minor effects on the results.

Longitudinal waves originating in the San Bernardino Mountain region have been observed (Gutenberg, 1941) to arrive at Pasadena slightly north of east rather than along a direct path from the east. The waves appear to have been diverted a little north of a direct path, possibly because of the presence of a higher velocity there. Assumptions of direct travel paths between these epicenters and Pasadena should, therefore, introduce only very slight errors in the results.

2. Initial amplitude identifications on seismograms

SV and SH motions determined from initial amplitude observations on seismograms are usually in agreement with those expected from known southern California fault types. It appears, therefore, that amplitude measurements of the initial wave displacements were made rather than those of a later phase. The question arises whether

initial wave displacements from the more distant shocks are too weak to be recorded, in which case later phases might be mistaken for initial displacements. Initial shear motions on seismograms from 14 aftershocks of a quake at 130 km epicentral distance indicated, with few exceptions, the same SV and SH displacement directions. Since the smaller of this group of aftershocks show the same motions as the relatively larger ones, a reasonable generalization is that initial displacements were measured in even the more distant shocks.

Usually initial displacements on seismograms were readily discernible; doubtful measurements were not used.

3. Reliability of amplitude and period measurements

Amplitude measurements, even where small, are sufficiently accurate to indicate horizontal directions of displacement within ± 5 degrees. Periods of waves were measured to within 0.1 second. Insignificant errors for the purpose of this study are introduced by the readings.

4. Response of seismographs to ground transients

Berlage (1930) discusses responses of mechanical seismographs to harmonic transient impulses of the form

$$\xi = \xi_0 t e^{-at} \sin \omega t$$

for various frequency ratios. His results can be applied to torsion instruments, recording through optical systems. Berlage demonstrates that the initial phase of 0.5 second transients, an average in this

study, is recorded quite accurately by 0.8 second instruments. Ground transients are unlikely to be harmonic; therefore, torsion seismograph responses to actual transients can only be approximated by Berlage's results. Uncertainties in ground displacements are reduced by using amplitude ratios of horizontal instruments. Response of Benioff electromagnetic seismographs to transient inputs is a combination of velocity and displacement. Such responses are difficult to interpret.

5. Anisotropy in the upper crustal layers

Stoneley (1949), after the method of Rudzki (1911), pointed out that anisotropy in continental structures will result in differential SV and SH velocities. In anisotropic media five constants replace Lamé's λ and μ in isotropic media. It is observed that initial amplitudes of shear waves on the three component seismographs arrive within 0.2 seconds of one another, regardless of ray azimuths. Time differences of this magnitude are probably within the limits of error of recording. Anisotropy in the upper crust of southern California is apparently too small to be discernible on seismograms.

6. Reliability of Knott and Zoeppritz equations

The Knott and Zoeppritz equations are probably reliable for calculations of the partitioning of SH waves incident at the surface. The equations appear to be good approximations for incident SV waves, but they involve imaginary reflected compressional waves for the range of SV incidence angles

$$\sin^{-1} \frac{V_s}{V_p} < i_0 < \frac{\pi}{2}$$

where V_s and V_p are the shear and compressional wave velocities, respectively. The equations (Wiechert, 1907 or Gutenberg, 1944b) for these incidence angles are used with complex quantities. Should the equations be incorrect approximations, SV computations may be in error.

7. Variations in wave paths and depths of focus

Variations in focal depths encountered in southern California will not significantly alter incidence angle or corresponding SV determinations.

The greatest deviation in crustal structure from that of figure 9 lies in the Los Angeles Basin where large thicknesses of sediments overly older rocks. There is little question that some of the direct waves travelling across the basin and recorded in Pasadena pass through these sedimentary layers. Since thicknesses and velocities of the sediments are not known well, wave paths across the basin can only be surmised. One important effect of the sediments on waves is to increase angles of incidence at the surface: rays leaving the basin are refracted from lower velocity sediments into higher velocity granites as they approach Pasadena. The sedimentary beds probably have little effect on initial directions of SV and SH motions, although they probably do alter the magnitudes of SV and the ratio SV/SH.

In summary, it appears that direct SH vibrational directions determined are probably reliable; those of the SV waves may be subject to some uncertainty. Values of SV/SH calculations may be doubtful.

DISTRIBUTIONS OF OBSERVED SV AND SH MOTIONS

Initial directions of SH vibrations observed at Pasadena and Riverside (Figs. 10 and 11) indicate striking consistencies of motions within local regions. Directions of SV vibrations (Figs. 12 and 15) indicate considerably less consistencies of motions, although in several very localized regions some uniformity is apparent. SV/SH ratios generally vary considerably, but in a few localities some uniformity of values is also observed.

Vibrational directions of SV waves are known to be functions not only of horizontal fault components and ray azimuths, as are the SH waves (Figs. 4 through 8), but are also known to be functions of vertical fault displacements. Therefore, the observed discrepancies of the SV motions may result, in part, from inconsistent vertical components of faulting.

The uniformity of SH motions observed indicates that strongly preferred directions of horizontal fault components exist in southern California. The SV data indicate discordant vertical movements along faults in the same vicinity. Conformability of the SH motions also suggests that the SH waves are polarized. Polarization of the SV waves is not so clearly inferred, although some is suggested. It is plausible that the entire shear wave is approximately plane polarized.

Small fault displacements over limited fault surfaces can be considered as linear movements. Thus small faults resulting in the recorded SV and SH motions may be analyzed by comparing the observations with the theoretical vibration directions and corresponding fault movements (Figs. 4 through 8), if deviations from the assumptions listed on page 10 are properly evaluated. Since direct rays between the source and surface are refracted, the assumption of a straight line path must be modified; the other assumptions (p. 10) are generally adequate for the purposes of this research.

Refractions through the crustal layers result in a difference in incidence angles between the surface and source. Approximate incidence angles at the source, for rays travelling the postulated layers of the upper crust and originating at normal depths of focus, are shown in Figure 9. Energy losses of direct SV or SH waves from refractions at discontinuities in the crust are negligible (Gutenberg, 1944b, Fig. 1, p. 95) for the approximate velocity ratios and incidence angles involved. Thus neither directions nor magnitudes of direct SH waves should be appreciably altered by the horizontal refracting layers. SV directions are probably not altered substantially, although the ratio u/w does vary with incidence angle.

Direct rays originating at normal depths of focus will generally travel from a low velocity layer into an overlying one of higher velocity. Incidence angles at the source for such waves are calculated to be about 70° or less (Fig. 9). Such angles are comparable

to those on Figures 4 through 8. Direct waves travelling across the basin may, however, leave the source at larger incidence angles.

It can be concluded that observed SV and SH motions originating from faults may be simulated by the theoretical illustrations of Figures 4 through 8. The data can therefore be compared to these illustrations to determine possible related fault types. The theoretical figures may be used unamended, except for rays travelling across the basin. Minor effects on the vibrations of waves traversing the basin may be introduced by the sediments.

Tectonic interpretations of the data, discussed in the following, are based on a comparison of the SV and SH data with: (1) shear wave vibrational directions and corresponding fault types shown on Figures 4 through 8; and (2) impulses of compressional waves observed by Gutenberg (1941) from shocks in the same general regions as the present study.

Compressional impulses were not recorded in the present investigation. Those from Gutenberg's paper pertain to an earlier group of shocks (between 1934 and 1940) than the data of the present study (1941 to 1949). As all shocks during the period 1934 - 1949 undoubtedly resulted from similar regional stress distributions, compressional data from the earlier shocks can be used in conjunction with shear data from the more recent ones to describe related faulting.

In the following, fault types consistent with observed longitudinal and transverse wave impulses are described. Each epicenter used is designated by a letter and a number, as appearing both in Figures 10 through 15 and in the fundamental data. The letter refers to an area bounded by a degree of latitude and longitude. The numbers increase from south to north in each lettered region. In Figures 10 and 11, initial SH vibrations at Pasadena and Riverside are shown. In Figures 12 and 13, the initial motions of the horizontal component, u , of the SV waves recorded at the two stations are shown. In Figures 14 and 15, the initial vertical motions, w , of the SV waves and the ratios SV/SH observed at the two stations are given.

Region C: Group of shocks between Pasadena and Riverside.

At both Pasadena and Riverside the group of shocks between these stations are recorded with northerly SH motions, suggesting that the stations are both located on fault blocks moving relatively northward. SV motions, to the extent that they are significant, suggest that for some shocks the stations are located on the down-thrown fault block, and for others on the upthrown block. SV/SH ratios, of questionable reliability, suggest a wide range of fault dips. Seven shocks of this group were recorded at both Pasadena and Riverside. All seven indicated northerly SH displacements; four indicated the same SV directions, and three opposite directions. Similar SV/SH ratios were observed for two of the seven shocks at

both stations, but for the other five the ratios were markedly dissimilar. Differences in ratios at the stations were not consistent. Results from these seven shocks are in agreement with the relative consistencies in SH and SV motions and values of SV/SH expected (p. 30).

Initial impulses of compressional waves from this epicentral region (Gutenberg, 1941) usually arrive at Pasadena as compressions and at Riverside as dilatations (Figs. 16 and 17).

Faulting in the region consistent with the SH and P impulses is an approximately east west trending reverse or thrust type. SV and SV/SH data are generally in agreement with such faulting. San Andreas type of motion, a northwesterly trending right handed transcurrent movement, is not in agreement with the SH displacements recorded at Riverside. North of this group of shocks lies the San Andreas fault, probably defining the northerly limit of the ostensibly reverse or thrust type of movements.

It is notable that the above mentioned group of shocks recorded at the Pasadena station are wholly compatible with the San Andreas type of faulting; recordings at both Pasadena and Riverside were required to determine the fault types described.

Region E - F: South of Pasadena

The group of shocks south of Pasadena are generally recorded with southerly SH motions at both Pasadena and Riverside, indicating a

predominately southerly displacement of the fault block on which the stations are located. About 75% of the SV waves from these epicenters are recorded as up motions at Pasadena; most of the relatively few shocks from this region recorded at Riverside are down motions. Ratios SV/SH varied markedly and were quite erratic at both stations. Gutenberg noted that from these epicenters dilatations generally arrive at Pasadena and compressions at Riverside.

Fault patterns consistent with the data are not readily discernible. Of the common fault types, that most in agreement with the data is a slightly north of east trending reverse or thrust movement. The Norwalk fault may be one of such displacement. Generally San Andreas types of motion are not consistent with the SH data at Pasadena, although several scattered shocks in this region do suggest a few such displacements. Due east west reverse or thrust faults are not consistent with some of the P data at Riverside; northeasterly trending left handed transcurrent faulting is not in close agreement with SH data at that station. A majority of the data does not substantiate vertical, horizontal, or normal faulting.

Region E: Southwest of Pasadena

SH and SV motions from shocks southwest of Pasadena were studied only at the Pasadena station. SH motions indicate southerly displacements of the fault block on which Pasadena is located. SV motions are inconsistent. Longitudinal waves have been shown by Gutenberg to arrive as dilatations at Pasadena and compressions at

Riverside. Waves from many of these shocks recorded at Pasadena probably traversed the sediments of the Los Angeles Basin. No appreciable changes in SH motions resulting from the sediments are evidenced. SV data are too erratic to determine possible effects of the sediments on SV vibrational directions. Faulting consistent with both the compressional and shear wave data includes either northeasterly trending reverse movements or northwesterly trending San Andreas type of displacements.

Region A - B: Northwest of Pasadena

SH and SV data from shocks northwest of Pasadena were studied only at the Pasadena station. A majority of the SH motions have northerly components. SV values and ratios SV/SH are inconsistent. Longitudinal waves recorded at Pasadena are shown by Gutenberg to arrive usually as dilatations, although several compressions are observed. At Riverside both compressions and dilatations are recorded. From the data it would seem that more than one type of faulting is common. Some of the data is consistent with east west trending reverse or thrust faults, and some with northeasterly trending left handed transcurrent faults.

Region C - D - F - G: East and northeast of Riverside

Most SH motions from shocks east and northeast of Riverside are recorded with northerly components at Riverside. The relatively few SH data from this region studied at Pasadena indicate both northerly

and southerly motions. SV and SV/SH data are generally erratic at both stations. Gutenberg indicates that at Riverside longitudinal waves from this region are recorded predominately as compressions, although some arrive as dilatations. At Pasadena, the longitudinal waves usually arrive as compressions. Most of the data is consistent with the San Andreas types of faulting, although some, inconsistent with such movements, are in agreement with reverse or thrust faulting. Data from a group of 14 aftershocks of a quake near Cabazon, in the vicinity of where the San Andreas fault strikes approximately east west for a short distance, all suggest reverse or thrust faulting. Probably transcurrent and reverse fault types coexist in the general area east of Riverside.

Region F - G: Southeast of Riverside

SH and SV motions from shocks southeast of Riverside are studied at only the Riverside station. Most of the SH motions have southerly components, but several, particularly in the northern part of this region, have northerly motions. The SV waves from shocks in this region at more than about 50 km epicentral distances usually indicate consistent initial down motions and small SV/SH ratios. Longitudinal waves recorded at Pasadena, according to Gutenberg, arrive usually as compressions, and at Riverside as either compressions and dilatations. San Andreas types of movements are generally consistent with the data. Rays from such fractures travel along the general line of faulting toward the two stations. For such paths some of the variations observed in the data would be expected. The

rather unusual consistency in both the SV motions and in the small ratios of SV/SH are also in agreement with primarily horizontal faulting in northwesterly and southeasterly directions.

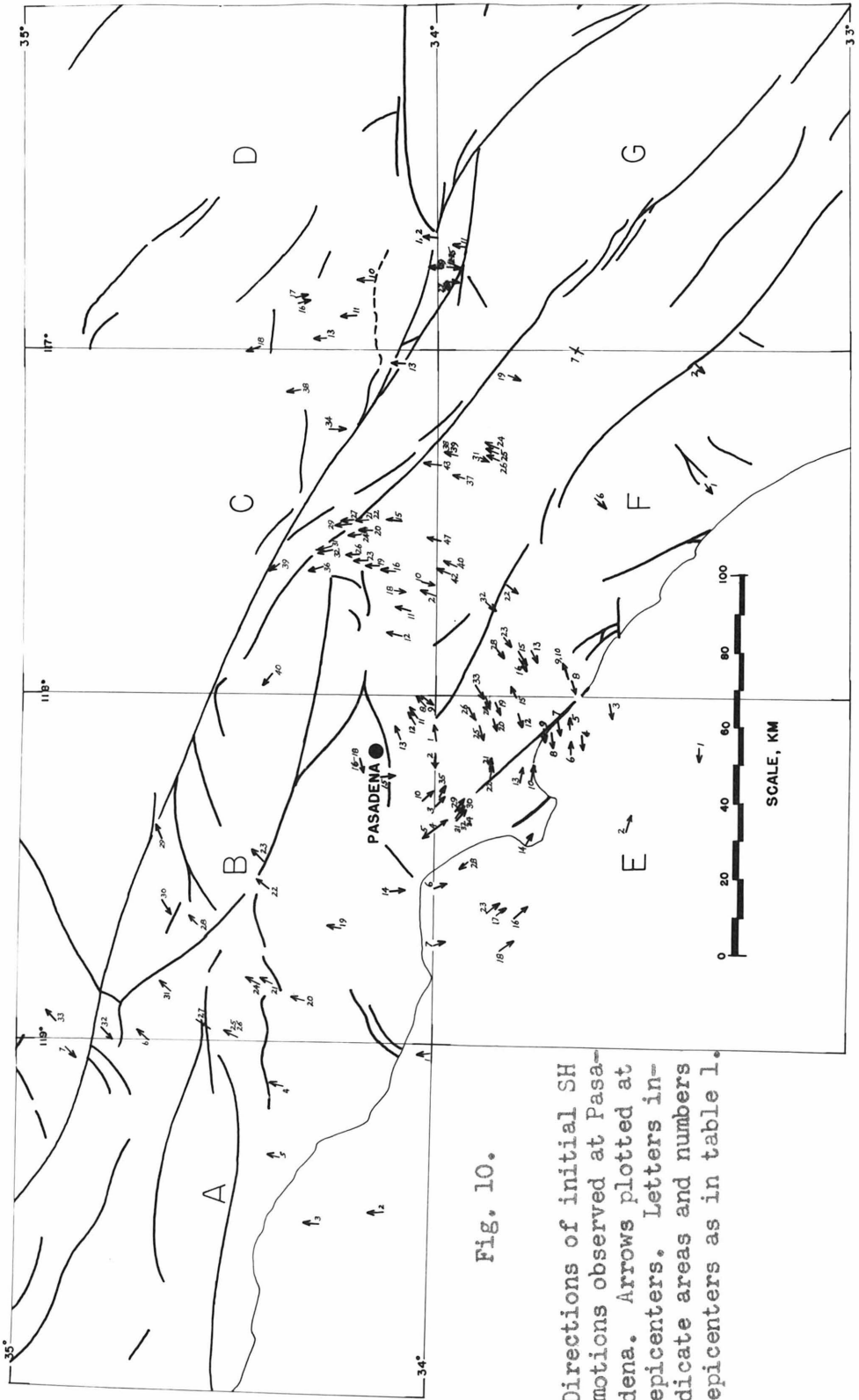


Fig. 10.

Directions of initial SH motions observed at Pasadena. Arrows plotted at epicenters. Letters indicate areas and numbers epicenters as in table 1.

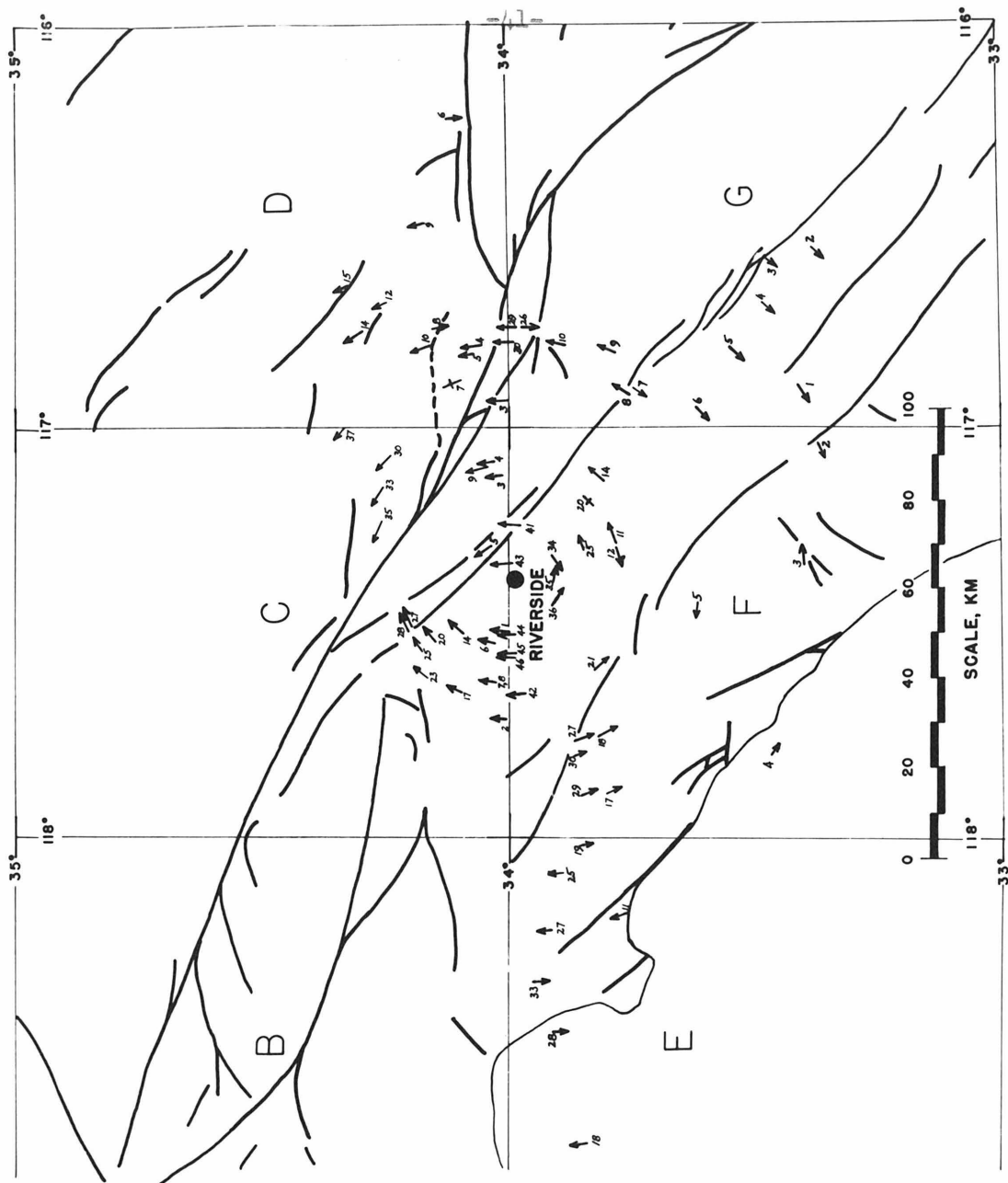


Fig. 11.

Directions of initial SH motions observed at Riverside. Arrows plotted at epicenters. Letters indicate area and numbers indicate epicenters as in table 1.

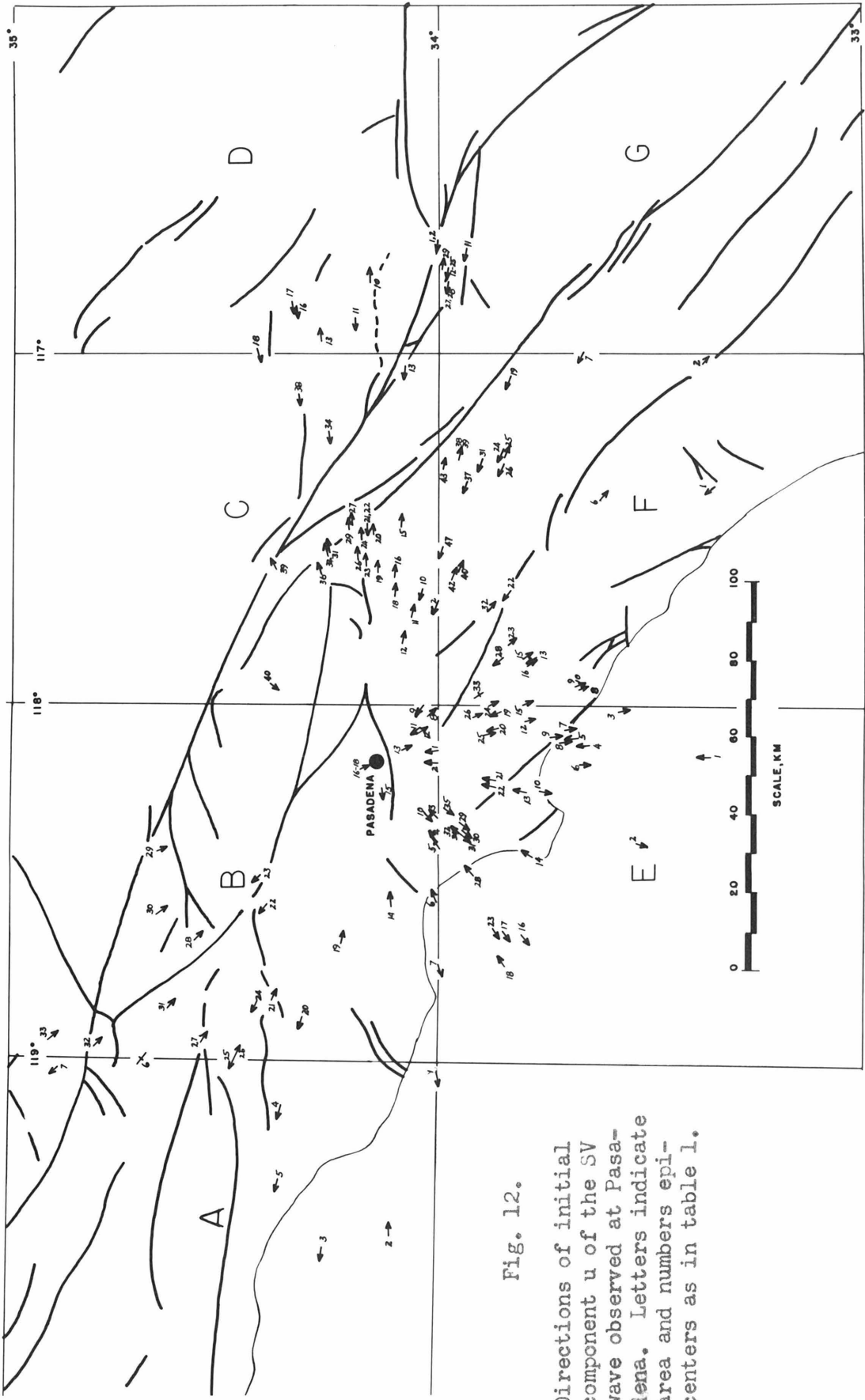


Fig. 12.

Directions of initial component u of the SV wave observed at Pasadena. Letters indicate area and numbers epicenters as in table 1.

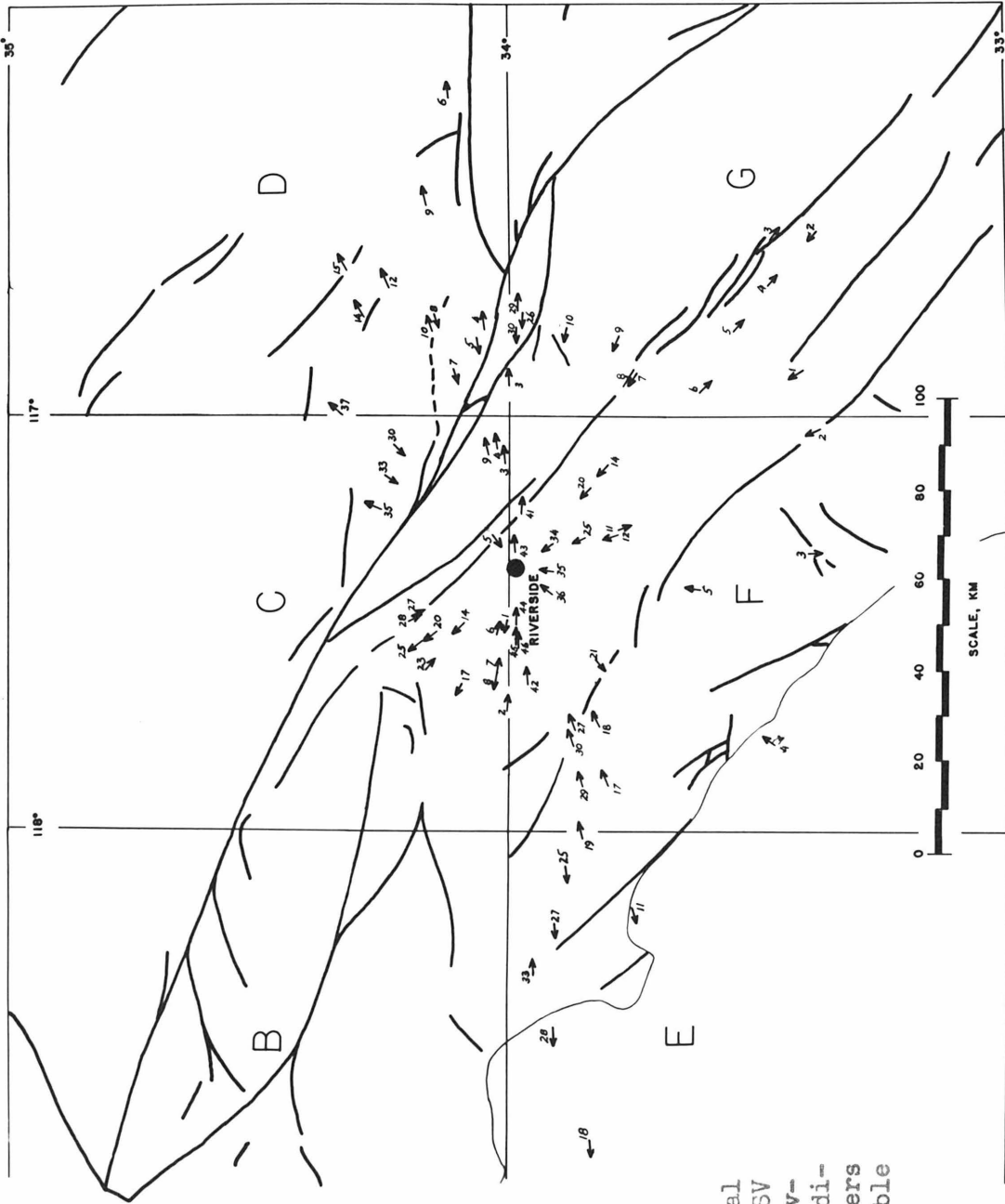


Fig. 13.

Directions of initial component u of the SV wave observed at Riverside. Letters indicate areas and numbers epicenters as in table 1.

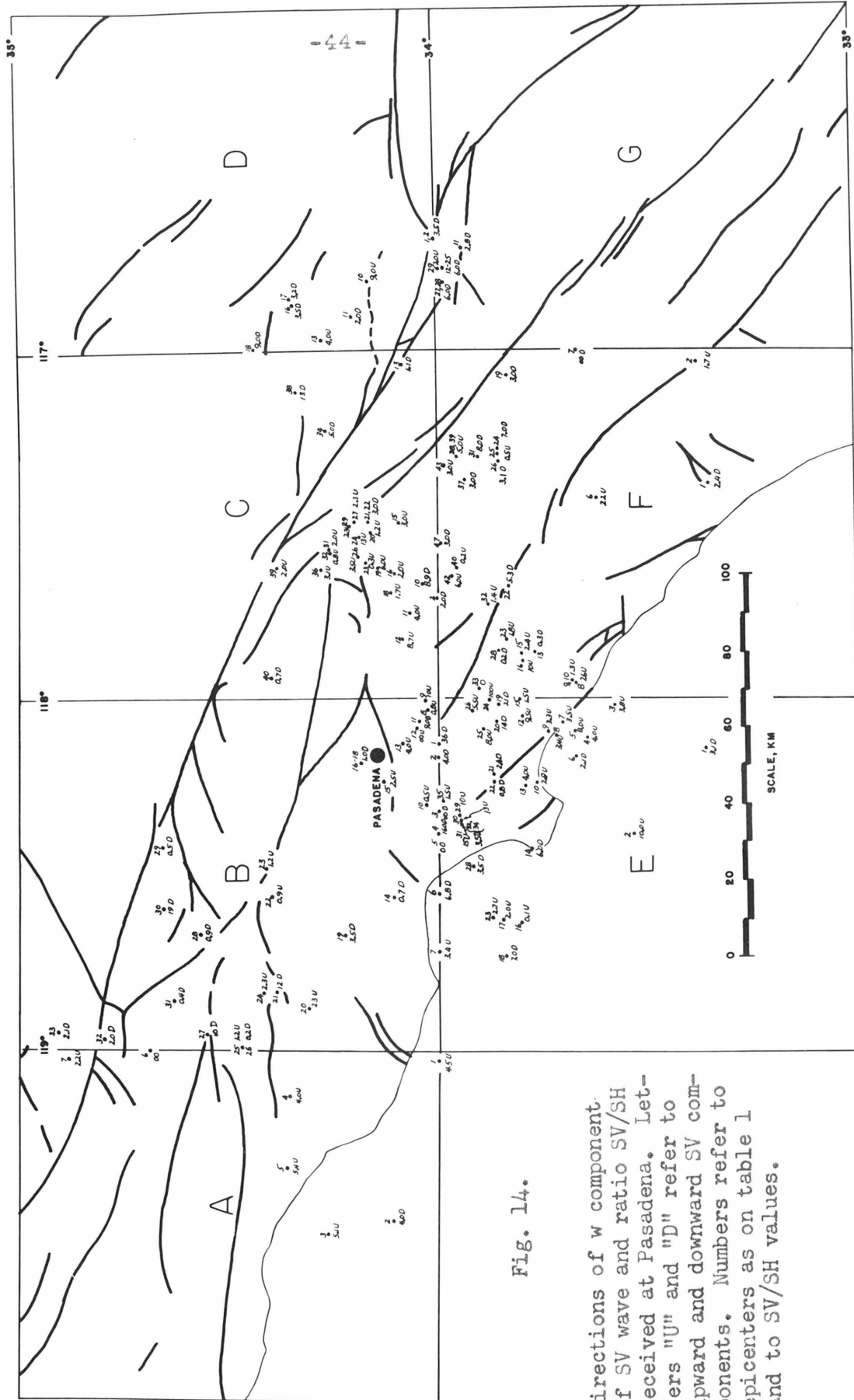


Fig. 14.

Directions of w component of SV wave and ratio SV/SH received at Pasadena. Letters "U" and "D" refer to upward and downward SV components. Numbers refer to epicenters as on table 1 and to SV/SH values.

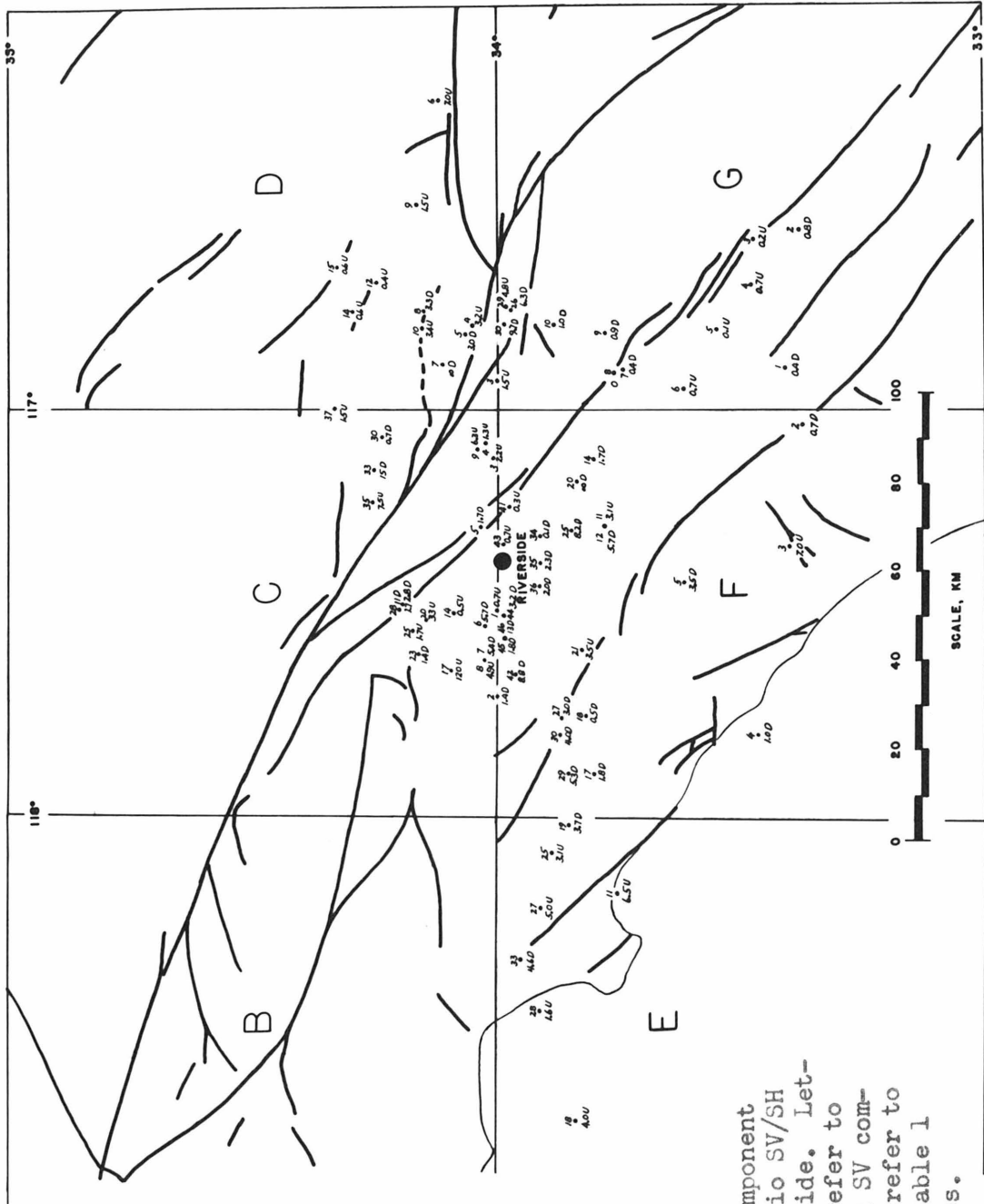


Fig. 15.

Directions of w component of SV wave and ratio SV/SH received at Riverside. Letters "U" and "D" refer to upward or downward SV components. Numbers refer to epicenters as on table 1 and to SV/SH values.

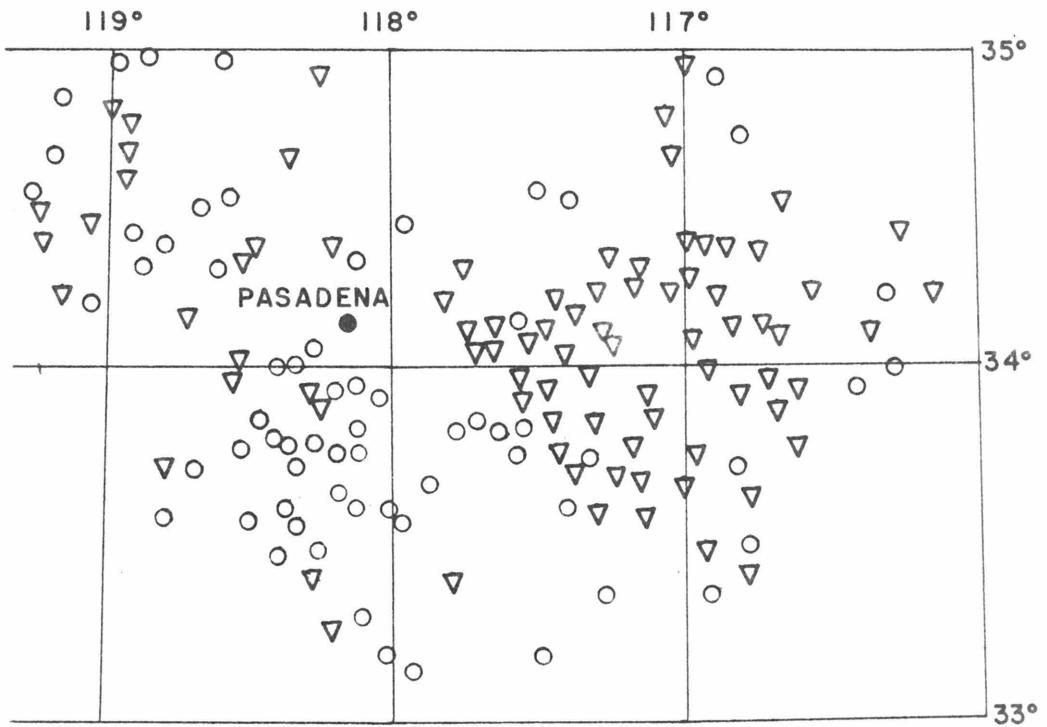


Fig. 16. Initial compressions (triangles) and dilatations (circles) received at Pasadena. Impulses plotted at epicenters. After Gutenberg, 1941.

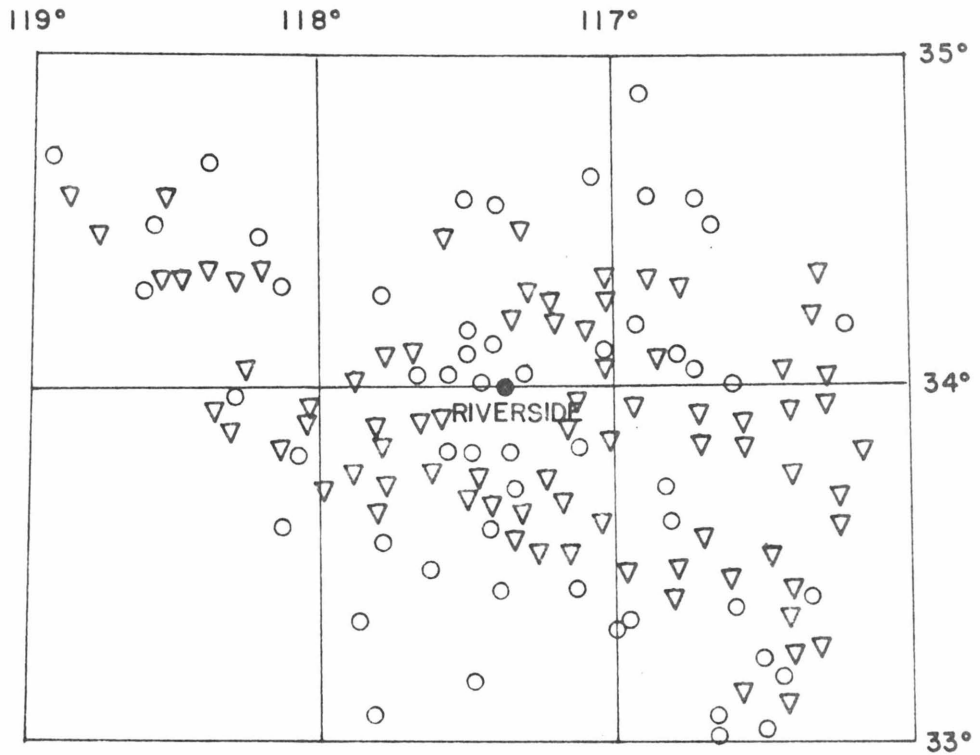


Fig. 17. Initial compressions (triangles) and dilatations (circles) received at Riverside. Impulses plotted at epicenters. After Gutenberg, 1941.

FAULT PATTERNS IN SOUTHERN CALIFORNIA

Seismological evidence for regional crustal structures and fault movements in southern California have been previously discussed by Gutenberg (1941, 1943) and Wood (1947). Particularly interesting are some of Gutenberg's (1941) findings on the impulses of longitudinal waves from shocks south of the Transverse Ranges. These impulses are usually consistent with northwesterly trending right handed transcurrent (strike slip) types of displacements (San Andreas type of movement) in which the southwesterly block moves relatively northwest. The results are reported rarely to be consistent with left handed motions along such faults.

Results from surface geologic mapping indicate that two types of faults have prevailed in the general vicinity of the Los Angeles Basin area of southern California.* One is a northwesterly trending movement of the San Andreas type and the other is an east west trending essentially vertical type of displacement. Such a fault pattern is fundamentally consistent with the seismic data obtained in this study and by Gutenberg (1941), suggesting that present day faulting may be very similar to that of the recent geologic past.

In some parts of southern California it appears that one or the other of these two fault types prevails, although there are some regions in which both appear to exist. A regional distribution of

* Oral communication, Dr. J. P. Buwalda.

of the fault types in agreement with the seismic data may be:

1. Transcurrent displacements trending northwesterly occur along the San Andreas fault and northeast and southeast from Riverside. East of Riverside, in the vicinity of Cabazon, the data indicate that in addition to transcurrent movements numerous east west trending reverse or thrust faults may exist. In this region the San Andreas fault strikes approximately east west for a short distance. It may well be that displacements in this portion of the San Andreas fault itself are primarily vertical rather than in the usual horizontal direction. Initial motions of a series of aftershocks from this region are all consistent with reverse or thrust movements. Southwest of the Los Angeles Basin either reverse, thrust, or San Andreas types of displacements are in agreement with the data.
2. Reverse or thrust faults trending east west, with some variations in strike, appear to prevail in most of the Los Angeles Basin. Known displacements of this type in the vicinity of the basin include the Whittier, Norwalk, and Foothill faults. Approximate dips of individual fault planes cannot be determined as the SV and SV/SH data are not consistent. Probably the dips vary; some may be low angle, although many, from the overall average SV/SH ratios appear to be high angle. Northerly fault dips are suggested by the SV data from some shocks and southerly from others.

3. Coexistence of east west trending reverse faults and northeasterly trending transcurrent faults is indicated in the Transverse Ranges northwest of Pasadena. Most of the transcurrent faults would appear to be left handed, i.e., the northwest block moves relatively southwest. Few data are in agreement with northwest trending right handed San Andreas types of movement.

POSSIBLE STRESS DISTRIBUTIONS IN SOUTHERN CALIFORNIA

The source of stresses acting in southern California is not known, but, as pointed out by Gutenberg (1941), it is probably related to differences in the Pacific and Continental structures in the crust. Regional stress distributions resulting from the observed fault pattern and consistent with the seismic data can, however, be postulated very generally.

One approximation to a stress distribution in southern California (Gutenberg, 1941) involves essentially shearing stresses acting, at depth, in a northwest southeast direction. A different type of distribution, involving principally compressional stresses, can also describe the overall fault pattern. Such a distribution, undoubtedly modified by complications at depth, is discussed in the following.

All of the fault types mentioned in this paper could be produced by a maximum principal stress acting in a north south direction. The strikes of both the transcurrent and thrust faults are in agreement with principal stresses directed very roughly north south, east west, and vertical. Variations from these directions may be appreciable in the mountainous regions.

Anderson (1942) has pointed out (see Terzaghi, 1943, for generalized theory) that east west trending thrust faults may result if

$$\sigma_N > \sigma_E > \sigma_V$$

where σ_N is the north south principal stress, σ_E the east west, and σ_V the vertical principal stress, and that northwesterly and northeasterly trending transcurrent faulting results if

$$\sigma_N > \sigma_V > \sigma_E$$

The intermediate principal stress lies in the fault plane. When the horizontal principal stresses are nearly equal but larger than the vertical, then (see Anderson) irregular striking thrust faults occur; i.e.

$$\sigma_N \sim \sigma_E > \sigma_V$$

When the vertical principal stress and one of the horizontal principal stresses are nearly equal, but smaller than the other principal stress, thrust and transcurrent faulting may coexist; e.g.

$$\sigma_N > \sigma_V \sim \sigma_E$$

A very generalized stress distribution in southern California roughly consistent with the seismic data may thus be postulated as:

1. In the region of the San Andreas fault northeast and southeast of Riverside, and possibly also in the region southwest of the Los Angeles Basin:

$$\sigma_N > \sigma_V > \sigma_E$$

2. East of Riverside where the San Andreas fault strikes east west for a short distance, and in the Transverse Ranges northwest of Pasadena:

$$\sigma_N > \sigma_E \sim \sigma_V$$

3. In most of the Los Angeles Basin as far east as Riverside, and particularly in the region between Riverside and Pasadena:

$$\sigma_N > \sigma_E > \sigma_V$$

Variations in the strikes of these faults, in so far as they exist, suggest that in this region σ_N may not be much larger than σ_E .

Complications at depth undoubtedly alter these oversimplified stress distributions. For example, the angles between the northwesterly and northeasterly trending transcurrent faults, as evidenced between the San Andreas and Garlock faults, are usually larger than would be consistent with this simple picture. Also, although thrust faults are readily explainable by this stress distribution, reverse faults may involve additional stresses. The assumed stress picture postulates complementary systems of faults. From surface geology it

appears that one set of these complementary systems is considerably more active than the other, indicating that other crustal stresses are probably also effective. Nonetheless, the overall fault pattern in southern California is essentially consistent with a stress distribution in which a north south principal stress direction is a maximum, and in which, in some areas, $\sigma_E > \sigma_V$, in others $\sigma_E \sim \sigma_V$, and in still others, $\sigma_E < \sigma_V$.

APPENDIX

DETERMINATION OF SHEAR WAVE STRAINS

Linear ground strains created by seismic disturbances can be determined approximately with Benioff strain seismometers. The accuracy of the approximations depends on the frequencies of the seismometer rod, recording galvanometer, and the ground disturbance. Expressions for strains of incident transverse waves will be derived in the following.

Let it be assumed that plane shear waves arrive at the instrument. They will give rise to a horizontal displacement

$$\bar{E}_g \quad \text{where} \quad \bar{E}_g = \sqrt{u_g^2 + v_g^2}$$

Following the analysis of Benioff (1935), the component of ground displacement parallel to the instrument rod (Fig. 18) is

$$\bar{E}_g \cos \gamma$$

where the angle γ is measured in a clockwise direction between the instrument and the direction of horizontal ground displacement. Let x be the direction of the rod. The linear ground strain at x is

$$\frac{d\bar{E}_g}{dx} \cos \gamma$$

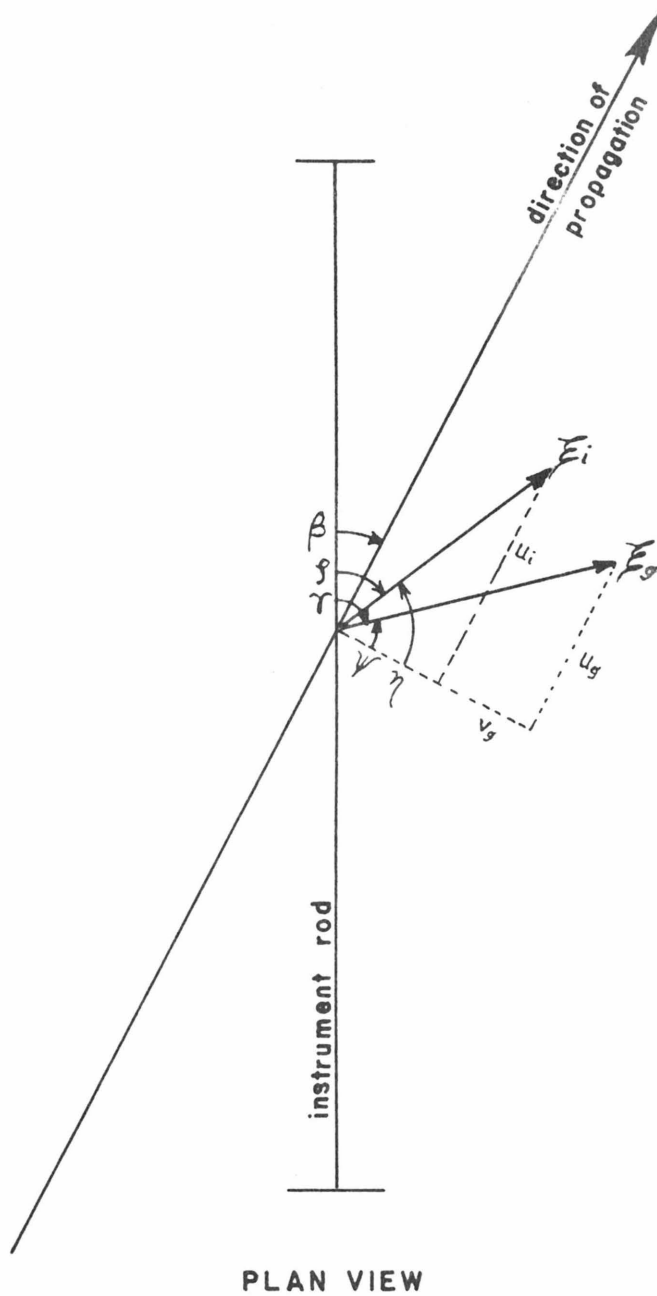


Fig. 18. Relationship between strain seismograph orientation, horizontal direction of shear wave propagation, and horizontal components of ground and incident wave displacements.

The displacement between the instrument piers, separated a distance L , is then

$$\Delta = \int_0^L \frac{\partial \xi_g}{\partial x} \cos \gamma dx \quad (5)$$

When the ground waves (plane) are long compared to the length of the instrument rod, γ and $\partial \xi_g / \partial x$ are approximately constant. The strain between the seismometer piers is then

$$\frac{\Delta}{L} = \frac{\partial \xi_g}{\partial x} \cos \gamma \quad (6)$$

Benioff (1935) has shown, for ground displacement of the form

$$\xi_g = \phi (t - r/c) \quad (7)$$

where r is the coordinate in the line of propagation and c is the apparent velocity, that

$$\frac{\partial \xi_g}{\partial x} = - \frac{\cos \beta}{c} \frac{\partial \xi_g}{\partial t} \quad (8)$$

β being the angle, measured clockwise from the instrument, between the rod and direction of propagation. A linear strain between the

instruments piers is now, by substitution,

$$\frac{\Delta}{L} = -\frac{\cos \beta \cos \gamma}{c} \frac{d\ddot{x}_g}{dt} \quad (9)$$

Since (Fig. 18)

$$\gamma = \left(\frac{\pi}{2} + \beta + \psi \right) \quad (10)$$

equation (9) can be written as

$$\frac{\Delta}{L} = \frac{\cos \beta \sin(\beta + \psi)}{c} \frac{d\ddot{x}_g}{dt}$$

Ground displacements u_g and v_g , determined from pendulum instrument records, are related to the angle ψ by

$$\psi = \tan^{-1} \frac{u_g}{v_g} \quad (11)$$

Strain measurements of incident transients necessitate seismographs that respond directly to ground displacement. Instruments now in use at Pasadena do not have such a response to short period transients. However, Benioff has designed a new transducer, which, used

on a strain seismograph recording through an 0.1 second galvanometer, measures ground displacements of all periods greater than about 0.2 to 0.3 seconds. Amplitudes written on seismograms by strain instruments with such transducers and short period galvanometers are proportional to ground strains, viz.

$$Z = K \left(\frac{\Delta}{L} \right) \quad (12)$$

where K is a proportionality factor. Substituting

$$Z = K \frac{d\bar{\epsilon}_g}{dX} \cos \gamma$$

or

$$Z = -K \frac{d\bar{\epsilon}_g}{dX} \sin (\beta + \psi) \quad (13)$$

For two strain instruments oriented perpendicularly in the directions x_1 and x_2

$$Z_1 = K_1 \frac{d\bar{\epsilon}_g}{dX_1} \cos \gamma \quad (14)$$

$$Z_2 = K_2 \frac{d\bar{\epsilon}_g}{dX_2} \cos \gamma'$$

defining

$$\gamma' = \gamma - \frac{\pi}{2} \quad (15)$$

and substituting gives

$$\begin{aligned} z_1 &= -K_1 \frac{\partial \xi_g}{\partial x_1} \sin(\beta + \psi) \\ z_2 &= K_2 \frac{\partial \xi_g}{\partial x_2} \cos(\beta + \psi) \end{aligned} \tag{16}$$

Horizontal components of ground and incident displacements can be related by the equations (Fig. 18)

$$\begin{aligned} \cos \psi &= v_g / \xi_g \\ \cos \eta &= v_i / \xi_i \end{aligned} \tag{17}$$

where u_i, v_i , and ξ_i refer to incident motions, and

$$\eta = \tan^{-1} \frac{u_i}{v_i}$$

At the earth's surface incident SH displacements are related to ground displacements, using the Knott and Zoeppritz equations, such that v_i equals half v_g ; i.e.

$$\begin{aligned} \xi_i \cos \eta &= \frac{1}{2} \xi_g \cos \psi \\ \xi_g &= 2 \left(\frac{\cos \eta}{\cos \psi} \right) \xi_i \end{aligned} \tag{18}$$

Since angles η and ψ are constant for plane waves,

$$\begin{aligned}\frac{d\tilde{\xi}_y}{dX_1} &= 2 \left(\frac{\cos \eta}{\cos \psi} \right) \frac{d\tilde{\xi}_i}{dX_1} \\ \frac{d\tilde{\xi}_y}{dX_2} &= 2 \left(\frac{\cos \eta}{\cos \psi} \right) \frac{d\tilde{\xi}_i}{dX_2}\end{aligned}\tag{19}$$

Substituting

$$\begin{aligned}Z_1 &= -2K_1 \sin(\beta + \psi) \left(\frac{\cos \eta}{\cos \psi} \right) \frac{d\tilde{\xi}_i}{dX_1} \\ Z_2 &= 2K_2 \cos(\beta + \psi) \left(\frac{\cos \eta}{\cos \psi} \right) \frac{d\tilde{\xi}_i}{dX_2}\end{aligned}$$

Transposing and writing k for $1/(2K)$

$$\begin{aligned}\frac{d\tilde{\xi}_i}{dX_1} &= k_1 \left(\frac{-\cos \psi}{\sin(\beta + \psi) \cos \eta} \right) Z_1 \\ \frac{d\tilde{\xi}_i}{dX_2} &= k_2 \left(\frac{\cos \psi}{\cos(\beta + \psi) \cos \eta} \right) Z_2\end{aligned}\tag{20}$$

Incident shear wave strains are (Fig. 18):

$$\begin{aligned}\left(\frac{\Delta_1}{L_1} \right)_i &= \frac{d\tilde{\xi}_i}{dX_1} \cos \rho = -\frac{d\tilde{\xi}_i}{dX_1} \sin(\beta + \eta) \\ \left(\frac{\Delta_2}{L_2} \right)_i &= \frac{d\tilde{\xi}_i}{dX_2} \cos \rho' = \frac{d\tilde{\xi}_i}{dX_2} \cos(\beta + \eta)\end{aligned}\tag{21}$$

where $\rho = \left(\frac{\pi}{2} + \beta + \eta \right)$

and $\rho' = \rho - \frac{\pi}{2}$

Incident strains can then be written as

$$\left(\frac{\Delta_1}{L_1} \right)_i = k_1 \left(\frac{\sin(\beta + \eta) \cos \psi}{\sin(\beta + \psi) \cos \eta} \right) z_1,$$

$$\left(\frac{\Delta_2}{L_2} \right)_i = k_2 \left(\frac{\cos(\beta + \eta) \cos \psi}{\cos(\beta + \psi) \cos \eta} \right) z_2$$

Simplifying gives

$$\left(\frac{\Delta_1}{L_1} \right)_i = k_1 \left(\frac{1 + \cot \beta \tan \eta}{1 + \cot \beta \tan \psi} \right) z_1,$$

(22)

$$\left(\frac{\Delta_1}{L_1} \right)_i = k_2 \left(\frac{1 - \tan \beta \tan \eta}{1 - \tan \beta \tan \psi} \right) z_2$$

Total horizontal incident strains can readily be calculated from these strain components.

REFERENCES

- Anderson, E. M.
1942. The dynamics of faulting, London, Oliver and Boyd.
- Benioff, H.
1935. "A linear strain seismograph", Bull. Seism. Soc. Am., vol. 25, pp. 283-309
- Berlage, H. P.
1930. "Seismometer", Handbuch der Geophysik (Ed. by B. Gutenberg), Band 4, Lieferung 2, pp.299-526, Berlin.
- Bullen, K. E.
1947. Introduction to the theory of seismology, Cambridge University Press.
- Geiger, L., and B. Gutenberg
1912. "Ueber Erdbebenwellen, VI.", Nachr. Gesell. d. Wiss. Göttingen, math.-phys. Kl., pp. 623-675
- Gutenberg, B.
1929. Handbuch der Geophysik, Band 4, Lieferung 1, pp. 1-298.
1941. "Mechanism of faulting in southern California indicated by seismograms", Bull. Seism. Soc. Am., vol. 31, pp. 263-302.
1943. "Earthquakes and structure in southern California", Bull. Geol. Soc. Am., vol. 54, pp. 499-526.
1944a. "Travel times of principal P and S phases over small distances in southern California", Bull. Seism. Soc. Am., vol. 34, pp. 13-32.
1944b. "Energy ratios of reflected and refracted seismic waves", Bull. Seism. Soc. Am., vol. 34, pp. 85-102.
1944c. "Reflected and minor phases in records of near-by earthquakes in southern California", Bull. Seism. Soc. Am., vol. 34, pp. 137-160.
1945. "Variations in physical properties within the earth's crustal layers", Am. Jour. Sci., vol. 243 A (Daly Volume), pp. 285-312.
1950. "Revised travel times in southern California", Bull. Seism. Soc. Am., (in print).
- Honda, H.
1932. "On types of seismograms and mechanism of deep earthquakes", Geophysical Mag., Tokyo, vol 5, pp. 301-326.

- Jeffreys, H.
1926. "The reflexion and refraction of elastic waves", Mon. Not. Roy. Astron. Soc., Geophys. Suppl., vol. 1, pp. 321-334.
- Kawasumi, H.
1933. "Study on propagation of seismic waves", Bull. Earthqke. Res. Inst., Tokyo, vol. 11, pp. 403-453.
1934. "Study on propagation of seismic waves", Bull. Earthqke. Res. Inst., Tokyo, vol. 12, pp. 660-705.
1937. "An historical sketch of the development of knowledge concerning the initial motion of an earthquake", Publications du Bureau Central Seismologique International (A) Travaux Scientifiques, vol. 15, pp. 258-330.
- Kawasumi, H., and R. Yosiyaama
1935. "On elastic waves animated by potential energy of initial strain", Bull. Earthqke. Res. Inst., Tokyo, vol. 13, pp. 496-503.
- Knott, C. G.
1899. "Reflexion and refraction of elastic waves, with seismological applications", London, Edinburg, and Dublin Philosophical Magazine and Journal of Science (5), vol. 48, pp. 64-97.
- Richter, C. F.
1935. "An instrumental earthquake magnitude scale", Bull. Seism. Soc. Am., vol. 25, pp. 1-32.
- Rudzki, M. P.
1911. "Parametrische Darstellung der Elastischen Welle in Anisotropen Medien", Bulletin de l'Academie des Sciences de Cracovie, pp. 503-506. (Taken from a review by F. Pockels in Gerlands Beiträge zur Geophysik, vol. 12 (1913), pp. 75-79.)
- Sezawa, K., and K. Kanai
1936. "Polarization of elastic waves generated from a plane source", Bull. Earthqke. Res. Inst., Tokyo, vol. 14, pp. 489-505.
- Stoneley, R.
1949. "Seismological implications of anisotropy in continental structures", Mon. Not. Roy. Astron. Soc., Geophys. Suppl., vol. 5, pp. 343-353.
- Terzaghi, K.
1943. Theoretical soil mechanics, New York.

Wiechert, E.

1907. "Ueber Erdbebenwellen I", Nachr. d. Wiss., Göttingen, math.-phys. Kl., pp. 415-529.

Wood, H. O.

1947. "Earthquakes in southern California with geological relations", Bull. Seism. Soc. Am., vol. 37, part 1, pp. 107-157, part 2, pp. 217-256.

Zoeppritz, K.

1919. "Ueber Erdbebenwellen VIIB", Nachr. d. Wiss., Göttingen, math.-phys. Kl., pp. 66-84.

Zoeppritz, K., L. Geiger, and B. Gutenberg

1912. "Ueber Erdbebenwellen V", Nachr. d. Wiss. Göttingen, math.-phys. Kl., pp. 121-206

BASIC DATA

The basic data and the initial vibrational displacements in the directions u, v, and w are shown on the following pages, each shock identified by letter and number corresponding to those in figures 10 through 15. Latitudes and longitudes of epicenters, origin times, and magnitudes of the shocks used were determined by the Pasadena seismological laboratory staff. Origin times are given by year, month, day, hour, and minute. Ground amplitude measurements are given in microns; periods of the waves in seconds.

Seismograms measured are denoted by three letters: T or B, for torsion or Benioff seismograph; S or L, for short or long period instrument; and N or E, for north south or east west component instrument. Thus TSE indicates the east west component of the short period torsion seismograph.

Most of the observations were made on the torsion seismograms. Although only one set of measurements at each station are listed on the data sheets, amplitude measurements frequently were made on seismograms at Pasadena from the horizontal torsion and/or the horizontal and vertical Benioff instruments. Torsion seismogram readings, when they were obtained, were used in preference to those of other seismograms.

Initial displacement directions are indicated by the components u, v, and w. A plus u is in the direction of epicenter to station; a plus v is rotated 90° clockwise from a positive u; and w is indicated

by "U" for an up motion, and "D" for a down motion.

A sample calculation will illustrate the method of determining vibrational directions. For the shock G 2, amplitude readings are $.70 \mu$ south on TSN and $.45 \mu$ west on TSE. The resolved total horizontal ground displacement is accordingly $.83 \mu$, in a direction rotated 212° clockwise from north. The ray azimuth is 313° clockwise from north. The vibration direction of the shear wave is then $313^\circ - 212^\circ$ or 101° clockwise rotation from the direction of propagation.

Components in the line of propagation, u_g , and normal to the direction, v_g , can be resolved from the total horizontal displacement ($.83 \mu$), giving $u_g = -.16 \mu$ and $v_g = -.81 \mu$.

Assuming a normal depth of focus and a layered crust according to Gutenberg's (1941) findings, the incidence angle for such an epicentral distance (Fig. 9) is 64° . SV calculations based on curves of u_g/SV vs i_0 (Gutenberg, 1944b, fig. 3b, p. 99) indicate that the incident SV amplitude is $+.32 \mu$, where the plus refers to the sign of the direction u . The SH amplitude, half the magnitude of v_g is -41μ . The ratios $SV/SH = 0.8$. Thus v_1 is -, u_1 is + and w_1 is down.

No.	Lat Long	Day Time	M.	Sta Dist	Inst	Ampl	Per	v	u	w	SV/SH
G											
1	33 25 116 57	49-1-22 13:15	3.2	R 77	TSN TSE	.45S .53W	0.4 0.3	-	+	D	0.4
2	33 26 116 13	48-6-20 13:29	3.5	R 100	TSN TSE	.70S .45W	0.5 0.5	-	+	D	0.8
3	33 29 116 35	49-2-5 22:24	3.0	R 93	TSN TSE	.21S .25W	0.6 0.5	-	-	U	0.2
4	33 29 116 42	48-12-28 04:53	4.0	R 84	TSN TSE	.53S .70W	0.5 0.5	-	-	U	0.7
5	33 33 116 50	45-9-22 01:05	3.8	R 72	TSN TSE	.87S 1.1W	0.3 0.3	-	-	U	0.1
6	33 37 116 57	47-8-27 23:59	3.2	R 57	TSN TSE	.42S .56W	0.4 0.4	-	-	U	0.7
7	33 45 116 54	49-1-8 22:21	2.4	R 50	TSN TSE	.35S .18W	0.5 0.5	-	+	D	0.4
8	33 45 116 55	48-9-16 11:22	3.2	R 49	TSN TSE	.28N .18E	0.3 0.3	+	0	0	0
9	33 47 116 50	47-10-6 06:18	2.6	R 56	TSN TSE	.18N .14E	0.4 0.4	+	+	D	0.9
10	33 53 116 44	47-8-9 07:12	2.9	R 54	TSN TSE	.18N .11E	0.3 0.3	+	+	D	1.0
11	33 55 116 42	43-11-17 03:28	4.5	P 138	TSN TSE	.70N .70E	0.5 0.4	+	+	D	2.8
12	33 58 116 45	44-6-12 02:50	3.7	P 130	TSN TSE	.35S .28E	0.5 0.4	-	+	D	43
13	33 58 116 45	44-6-12 03:13	3.5	P 130	TSN TSE	.18S .18E	0.4 0.4	-	+	D	5.7
14	33 58 116 45	44-6-12 05:45	3.8	P 130	TSN TSE	.60S .45E	0.5 0.4	-	+	D	5.8
15	33 58 116 45	44-6-12 06:43	3.5	P 130	TSN TSE	.10S .18E	0.4 0.4	-	+	D	10

No.	Lat Long	Day Time	M.	Sta Dist	Inst	Ampl	Per	v	u	w	SV/SH
G											
16	33 58 116 45	44-6-12 12:22	3.6	P 130	TSN TSE	.10S .07E	0.4 0.4	-	+	D	3.6
17	33 58 116 45	44-6-12 14:21	4.2	P 130	TSN TSE	.70S .60E	0.4 0.4	-	+	D	4.5
18	33 58 116 45	44-6-13 09:30	3.7	P 130	TSN TSE	.10S .14E	0.4 0.4	-	+	D	10
19	33 58 116 45	44-6-13 10:37	3.3	P 130	TSN TSE	.18S .18E	0.4 0.4	-	+	D	4.1
20	33 58 116 45	44-6-13 17:21	3.3	P 130	TSN TSE	.21S .14E	0.4 0.4	-	+	D	5.5
21	33 58 116 45	44-6-13 19:31	3.3	P 130	TSN TSE	.18S .18E	0.4 0.4	-	+	D	4.0
22	33 58 116 45	44-6-15 12:44	3.8	P 130	TSN TSE	.52S .45E	0.4 0.4	-	+	D	5.0
23	33 58 116 45	44-6-23 13:28	3.6	P 130	TSN TSE	.10N .14E	0.4 0.4	+	+	D	3.7
24	33 58 116 45	44-6-27 22:55	3.7	P 130	TSN TSE	.21S .35E	0.5 0.5	-	+	D	10
25	33 58 116 45	44-7-1 02:53	3.7	P 130	TSN TSE	.37S .28E	0.4 0.4	-	+	D	3.7
26	33 58 116 45	45-12-14 10:49	2.6	R 57	TSN TSE	.31S .25W	0.4 0.4	-	+	D	6.3
27	33 58 116 48	44-6-10 03:11	4.5	P 130	TSN TSE	3.7S 2.3E	0.3 0.4	-	+	D	3.4
28	33 58 116 48	44-6-10 03:15	4.0	P 130	TSN TSE	.46S .70E	0.3 0.3	-	+	D	9.4
29	33 59 116 46	48-4-29 13:45	3.5	P 130 R 56	TSN TSE TSN TSE	.14N .11E .45N .59W	0.4 0.4 0.4 0.4	+	-	U	2.0 4.8
30	33 59 116 52	45-9-7 07:45	3.0	R 53	TSN TSE	.35N .35E	0.4 0.4	+	+	D	9.7

No.	Lat Long	Day Time	M.	Sta Dist	Inst	Ampl	Per	v	u	w	SV/SH
F											
1	33 21 117 23	42-10-19 15:27	3	P 109	BSN BSE	.48S .24W	0.3 0.3	-	+	D	2.4
2	33 23 117 02	47-5-18 21:28	3.6	P 133 R 70	TSN TSE TSN TSE	.07S .14W .87S 1.4W	0.4 0.4 0.3 0.3	-	-	U D	1.7 0.7
3	33 25 117 20	47-9-6 08:48	2.9	R	TSN TSE	.42N .20E	0.3 0.3	+	-	U	7.0
4	33 28 117 48	48-6-24 10:06	3.8	R 69	TSN TSE	.70S .45W	0.5 0.5	+	+	D	1.0
5	33 37 117 24	48-4-5 02:28	3.0	R 42	TSN TSE	.70S .94W	0.3 0.3	-	+	D	3.5
6	33 37 117 24	48-4-5 02:28	3.0	P 90	BLN BLE	.33N .56W	0.5 0.5	-	-	U	22
7	33 40 117 00	43-4-15 23:04	3	P 117	BSN BSE	.09S .16E	0.3 0.3	0	+	D	∞
8	33 40 117 58	47-1-8 18:20	3.3	P 56	BLN BLE	1.3N .35W	0.5 0.6	-	-	U	26
9	33 41 117 57	48-3-3 11:32	2.8	P 55	TSN TSE	.21N .25E	0.6 0.5	+	-	U	1.3
10	33 41 117 57	45-2-17 12:09	3.2	P 60	TSN TSE	.35N .42E	0.6 0.4	+	-	U	1.2
11	33 47 117 17	46-12-30 10:57	2.7	R 24	TSN TSE	1.6N 1.2E	0.3 0.3	+	-	U	3.1
12	33 47 117 17	48-4-30 04:52	2.8	R 24	TSN TSE	.88S .52W	0.3 0.3	-	+	D	5.7
13	33 47 117 52	43-10-29 08:31	3.5	P 50	TSN TSE	.39S .49W	0.5 0.5	-	+	D	0.3
14	33 48 117 08	47-9-7 00:25	2.9	R 29	TSN TSE	.53N .94E	0.3 0.3	+	+	D	1.7
15	33 48 117 52	43-8-11 08:01	3	P 36	BLN BLE	.30S 1.1W	0.6 0.6	-	-	U	2.4

No.	Lat Long	Day Time	M.	Sta Dist	Inst	Ampl	Per	v	u	w	SV/SH
F											
16	33 48 117 53	47-8-18 11:56	2.8	P 44	BLN BLE	.40N .30W	0.6 0.6	-	-	U	10
17	33 48 117 53	47-8-18 11:56	2.8	R 48	TSN TSE	.21S 0	0.3 0.4	+	+	D	1.8
18	33 49 117 45	47-1-18 22:48	2.7	R 39	TSN TSE	.28S .11E	0.3 0.3	+	+	D	0.5
19	33 50 117 04	43-6-11 5:28	3.5	P 104	TSN TSE BLN	.28S .11E N	0.5 0.4	-	+	D	3.0
20	33 50 117 11	48-12-10 15:06	2.7	R 24	TSN TSE	.53S .53E	0.3 0.4	0	+	D	∞
21	33 50 117 35	49-1-26 11:12	2.3	R 26	TSN TSE	.28S .60E	0.3 0.3	+	-	U	3.5
22	33 50 117 40	44-9-20 08:35	3.4	P 60	TSN TSE	.42N .35W	0.4 0.4	-	+	D	5.3
23	33 50 117 50	44-12-13 15:51	3.4	P 46	TSN TSE	.86S 1.9W	0.4 0.3	-	-	U	1.8
24	33 51 117 17	47-11-7 19:02	3.1	P 86	BLN BLE	.30N .30E	0.6 0.6	+	+	D	7.0
25	33 51 117 20	48-10-6 12:16	3.1	P 82 R 17	TSN TSE TSN TSE	.21N .07E 4.7N 3.3E	0.4 0.3 0.2 0.3	+	-	U	0.5
								+	+	D	8.2
26	33 51 117 24	42-8-15 17:12	3.5	P 75	BLN BLE	.30N .60E	0.6 0.6	+	+	D	3.1
27	33 51 117 45	49-2-1 03:59	2.8	R 38	TSN TSE	.80S .28W	0.5 0.5	+	+	D	3.0
28	33 51 117 52	43-10-19 19:14	3	P 38	TSN TSE	.30S .20E	0.4 0.5	-	+	D	0.2
29	33 51 117 53	48-9-4 21:34	2.3	R 50	TSN TSE	.18S .18W	0.4 0.4	+	+	D	5.3
30	33 52 117 47	49-1-29 07:44	2.7	R 38	TSN TSE	.53S .25W	0.3 0.4	+	+	D	4.0

No.	Lat Long	Day Time	M.	Sta Dist	Inst	Ampl	Per	v	u	w	SV/SH
F											
31	33 53 117 18	46-4-19 07:55	3.4	P 85	TSN TSE	.21S .18E	0.5 0.5	-	+	D	8.0
32	33 53 117 43	44-7-25 00:20	3.0	P 49	TSN TSE	.18S .20W	0.5 0.4	-	-	U	1.4
33	33 54 117 58	49-1-30 16:21	2.4	P 32	TSN TSE	.11S .18W	0.4 0.4	-	0	0	0
34	33 55 117 19	48-3-15 19:46	3.1	R 9	TSN TSE	4.0S 10.7W	0.3 0.3	-	+	D	0.1
35	33 55 117 26	49-2-28 07:47	2.5	R 14	TSN TSE	1.8N 1.6E	0.2 0.2	+	+	D	2.3
36	33 55 117 26	48-4-16 06:28	2.5	R 10	TSN TSE	.88N 1.6E	0.5 0.5	+	+	D	2.0
37	33 56 117 22	43-10-23 16:29	4	P 76	TSN TSE	.52N .70E	0.4 0.5	+	+	D	3.0
38	33 57 117 18	45-11-8 03:19	3.5	P 82	TSN TSE	.35N .21W	0.6 0.6	+	-	U	4.0
39	33 57 117 18	45-11-8 05:06	3.3	P 82	TSN TSE	.21N .18W	0.6 0.6	+	-	U	6.0
40	33 57 117 37	43-7-4 13:53	3	P 54	TSN TSE	.63N .25E	0.4 0.4	+	-	U	0.2
41	33 58 117 14	47-1-8 05:24	3.0	R 12	TSN TSE	3.5N 1.7E	0.3 0.3	+	-	U	0.3
42	33 58 117 39	48-6-25 14:12	3.0	P 50 R 25	TSN TSE TSN TSE	.14N .11W 2.8N 1.4W	0.4 0.4 0.3 0.3	+	-	U D	6.0 8.8
43	33 59 117 20	47-6-25 04:30	3.2	P 78 R 3	TSN TSE TSN TSN	.18N .18W 6.7N 4.9E	0.4 0.4 0.3 0.3	+	-	U U	3.0 0.7
44	33 59 117 30	47-8-30 02:48	2.7	R 12	TSN TSE	.42N 1.2E	0.3 0.3	-	+	D	3.2
45	33 59 117 33	48-2-18 03:55	2.3	R 17	TSN TSE	1.1N 1.2E	0.3 0.2	-	+	D	13

No.	Lat Long	Day Time	M.	Sta Dist	Inst	Ampl	Per	v	u	w	SV/SH
F											
46	33 59 117 33	48-2-18 05:38	3.3	R 17	TSN TSE	18.0W 16.0E	0.2 0.2	-	+	D	1.8
47	33 59 117 33	48-2-18 05:38	3.3	P 58	TSN TSE	.21N .28E	0.6 0.6	+	+	D	3.0
E											
1	33 22 118 09	42-4-15 23:28	4	P 85	TSN TSE	.53S .70W	0.4 0.4	-	+	D	3.1
2	33 32 118 23	45-6-27 09:17	2.8	P 69	TSN TSE	.18N .10E	0.4 0.4	+	-	U	10
3	33 35 118 01	48-5-24 02:38	3.6	P 63	TSN TSE	.70N 1.1W	0.5 0.6	-	-	U	3.8
4	33 39 118 06	46-11-22 00:19	3.0	P 55	TSN TSE	.21S .18W	0.5 0.5	-	+	D	4.0
5	33 40 118 05	43-5-18 14:35	3	P 53	BLN BLE	1.8S 1.3E	0.6 0.6	+	+	D	8.0
6	33 40 118 09	43-5-17 11:21	3	P 52	BLN BLE	.65N 1.3E	0.6 0.6	+	-	U	2.1
7	33 42 118 06	44-8-15 22:32	3.5	P 48	TSN TSE	.46N .35W	0.4 0.4	-	-	U	3.5
8	33 43 118 10	44-10-23 14:00	3.6	P 44	TSN TSE	.35N .35W	0.4 0.4	-	-	U	3.4
9	33 44 118 09	44-1-14 00:08	3.3	P 46	TSN TSE	.20N .30W	0.5 0.5	-	-	U	3.3
10	33 45 118 14	44-7-26 14:59	3.8	P 40	TSN TSE	1.8S 1.0E	0.4 0.4	+	-	U	2.9
11	33 46 118 10	49-2-27 16:17	2.6	R 78	TSN TSE	.21N .18E	0.4 0.5	-	-	U	6.5
12	33 47 118 02	44-12-24 00:18	2.6	P 40	TSN TSE	.18N .11W	0.6 0.4	-	-	U	9.5
13	33 47 118 15	44-7-26 14:59	3.8	P 40	TSN TSE	1.8S 1.0E	0.4 0.4	+	+	D	4.0

No.	Lat Long	Day Time	M.	Sta. Dist	Inst	Ampl	Per	v	u	w	SV/SH
E											
14	33 47 118 25	42-2-26 17:28	3	P 46	TSN TSE	.18S 0	0.4 0.4	+	+	D	6.0
15	33 48 118 00	43-7-17 13:33	3	P 42	TSN TSE	.28N .35E	0.4 0.4	+	-	U	1.5
16	33 49 118 39	45-1-26 14:00	2.9	P 62	TSN TSE	.28S .21E	0.4 0.4	+	-	U	0.1
17	33 51 118 39	46-4-8 05:04	3.0	P 56	TSN TSE	.11S .21E	0.5 0.5	+	-	U	2.0
18	33 51 118 43	47-10-12 23:25	3.7	P 62 R 124	BLN BLE TSN TSE	2.0S .60W .88N .66E	0.6 0.6 0.4 0.3	+	+	D	7.0
								-	-	U	4.0
19	33 52 118 01	47-9-11 13:19	2.8	P 35 R 62	TSN TSE TSN TSE	.53N .35W .28S .18W	0.4 0.4 0.3 0.3	-	+	D	21
								+	+	D	3.7
20	33 52 118 03	44-4-19 22:02	2.9	P 35	TSN TSE	.30S 0	0.5 0.4	-	+	D	14
21	33 52 118 13	44-6-18 23:28	2.9	P 35	TSN TSE	.35S .35E	0.4 0.4	+	+	D	2.4
22	33 52 118 15	44-6-18 23:53	2.7	P 35	TSN TSE	.28S .56E	0.4 0.4	+	+	D	0.8
23	33 52 118 37	43-10-20 13:34	3	P 51	BLN BLE	.25S .70E	0.4 0.6	+	-	U	2.7
24	33 53 118 00	47-5-3 14:39	2.6	P 33	TSN TSE	.21N .14W	0.5 0.5	-	-	U	100
25	33 53 118 05	48-2-19 11:36	2.9	P 29 R 65	TSN TSE TSN TSE	.53N .46W .31N .14E	0.4 0.4 0.4 0.4	-	-	U	8.0
								-	-	U	3.1
26	33 55 118 02	46-7-3 15:40	2.5	P 27	TSN TSE	.17N .34W	0.4 0.4	-	-	U	5.5
27	33 55 118 13	48-2-19 20:21	3.6	R 78	TSN TSE	.35N .35E	0.3 0.3	-	-	U	5.0

No.	Lat Long	Day Time	M.	Sta Dist	Inst	Ampl	Per	v	u	w	SV/SH
E											
28	33 55 118 28	47-10-24 11:14	3.0	P 38	BLN BLE	.10N .30W	0.6 0.6	-	+	D	3.5
				R 101	TSN TSE	.35S .18E	0.3 0.3	+	-	U	1.6
29	33 56 118 19	45-1-18 21:10	3.5	P 30	TSN TSE	2.5N 3.7E	0.4 0.4	+	-	U	10
30	33 56 118 22	44-6-18 10:09	2.6	P 30	TSN TSE	.10N .10E	0.4 0.4	+	-	U	13
31	33 57 118 21	45-2-5 06:43	2.4	P 28	TSN TSE	.18N .28E	0.5 0.5	+	-	U	15
32	33 57 118 21	45-2-6 14:56	3.5	P 28	TSN TSE	2.6S 2.1E	0.4 0.4	+	+	D	5.3
33	33 57 118 21	47-6-16 07:59	2.8	P 89	TSN TSE	.18S .18W	0.4 0.5	+	+	D	4.6
34	33 57 118 21	45-2-7 01:11	2.6	P 27	TSN TSE	.63S .42E	0.4 0.4	+	+	D	1.5
35	33 59 118 18	43-9-23 5:21	2.5	P 20	TSN TSE	.88S 1.2E	0.3 0.3	+	-	U	1.5
D											
1	34 00 116 42	44-6-12 16:19	3.7	P 138	TSN TSE	.42S .35E	0.4 0.4	+	+	D	4.7
2	34 00 116 42	44-8-24 23:30	4.2	P 138	TSN TSE	.52S .52W	0.4 0.4	+	+	D	2.7
3	34 00 116 56	49-2-16 03:02	2.7	R 40	TSN TSE	.42N .17W	0.3 0.3	+	-	U	1.5
4	34 03 116 48	45-9-3 15:08	3.1	R 53	TSN TSE	.32N .35W	0.4 0.4	+	-	U	3.2
5	34 05 116 49	48-3-30 08:25	3.4	R 51	TSN TSE	1.1N .54E	0.3 0.3	+	+	D	3.0
6	34 07 116 14	48-2-28 09:24	3.6	R 103	TSN TSE	.35S .45E	0.4 0.4	-	-	U	7.0

No.	Lat Long	Day Time	M.	Sta Dist	Inst	Ampl	Per	v	u	w	SV/SH
D											
7	34 07 116 53	48-4-25 11:11	3.1	R 46	TSN TSE	.13N .35E	0.4 0.4	0	+	D	∞
8	34 09 116 45	49-3-23 15:33	3.1	R 59	TSN TSE	.25S .35E	0.4 0.4	-	+	D	3.3
9	34 10 116 30	48-11-11 16:25	3.6	R 82	TSN TSE	.63N .49W	0.4 0.4	+	-	U	1.5
10	34 10 116 48	48-7-30 09:24	3.6	P 123 R 55	TSN TSE TSN TSE	.14N .25W .70N 1.2W	0.5 0.5 0.4 0.5	+	-	U	9.0 3.4
11	34 12 116 54	45-3-27 10:41	3.5	P 116	TSN TSE	.45N .18E	0.5 0.4	+	+	D	2.0
12	34 15 116 41	47-8-29 11:09	3.4	R 69	TSN TSE	.32N .18W	0.4 0.4	+	-	U	0.4
13	34 16 116 58	43-8-28 19:57	4	P 112	TSN TSE	.88S 1.1E	0.4 0.4	+	-	U	4.0
14	34 18 116 45	47-3-10 21:50	3.0	R 66	TSN TSE	.28N .24W	0.4 0.4	+	-	U	0.6
15	34 20 116 39	47-8-31 18:26	3.4	R 76	TSN TSE	.45N .35W	0.5 0.5	+	-	U	0.6
16	34 20 116 53	43-10-14 06:28	4.5	P 115	TSN TSE	1.4S 1.4E	0.5 0.5	-	+	D	3.5
17	34 21 116 52	43-10-15 08:50	4.5	P 115	TSN TSE	.88S .88E	0.4 0.4	-	+	D	3.2
18	34 26 116 59	45-4-17 20:58	4.3	P 110	TSN TSE	.52N .35E	0.4 0.4	+	+	D	9.0
C											
1	34 00 117 30	47-5-28 14:41	2.4	R 12	TSN TSE	1.8N .88W	0.3 0.3	-	-	U	0.7
2	34 00 117 42	47-11-8 22:39	2.5	P 44	TSN TSE	.11N .11E	0.5 0.5	+	+	D	2.0

No.	Lat Long	Day Time	M.	Sta Dist	Inst	Ampl	Per	v	u	w	SV/SH
G											
2	34 00 117 42	47-11-8 22:39	2.5	R 32	TSN TSE	.42N .14W	0.2 0.3	-	+	D	1.4
3	34 01 117 07	48-8-31 21:58	2.7	R 23	TSN TSE	.88N .63W	0.3 0.3	+	-	U	2.2
4	34 02 117 05	49-1-3 12:07	2.8	R 27	TSN TSE	.46N .28W	0.4 0.4	+	-	U	1.3
5	34 02 117 17	48-5-31 03:30	2.6	R 9	TSN TSE	.88N 3.7W	0.3 0.3	+	+	D	1.7
6	34 02 117 32	48-2-1 11:46	2.2	R 15	TSN TSE	.98N 1.1E	0.3 0.3	-	+	D	5.7
7	34 02 117 38	45-10-15 05:59	2.7	R 25	TSN TSE	.88N .70W	0.3 0.3	-	+	D	5.4
8	34 02 117 38	48-4-19 00:09	2.3	R 23	TSN TSE	.32N .35E	0.4 0.4	-	-	U	4.9
9	34 03 117 06	45-11-19 01:38	2.5	R 25	TSN TSE	.28N .52W	0.3 0.3	+	-	U	6.3
10	34 03 117 40	44-7-9 08:42	2.9	P 48	TSN TSE	.20S .30E	0.4 0.4	-	+	D	8.9
11	34 04 117 45	46-7-1 23:28	3.2	P 38	TSN TSE	.70N .49W	0.4 0.4	+	-	U	4.0
12	34 04 117 49	48-7-17 17:03	3.6	P 31	TSN TSE	.80N 1.2W	0.5 0.5	+	-	U	8.7
13	34 05 117 02	45-6-17 01:03	3.4	P 102	TSN TSE	.07N .21W	0.4 0.4	+	+	D	1.1
14	34 05 117 30	47-12-30 12:48	2.4	R 17	TSN TSE	2.6N 1.4E	0.2 0.3	-	-	U	0.5
15	34 06 117 30	42-12-24 10:19	3	P 58	TSN TSE	.35N .21W	0.4 0.4	+	-	U	3.0
16	34 06 117 38	48-3-3 07:59	3.5	P 47	TSN TSE	1.4N .70W	0.4 0.5	+	-	U	2.0
17	34 06 117 38	48-3-3 07:59	3.5	R 28	TSN TSE	2.38 5.3E	0.3 0.3	-	-	U	120

No.	Lat Long	Day Time	M.	Sta Dist	Inst	Ampl	Per	v	u	w	SV/SH
18	34 117	43-2-11 05:54	2.5	P 48	TSN TSE	.18S .14W	0.4 0.4	-	-	U	1.7
19	34 08 117 37	48-10-2 15:07	3.4	P 50	TSN TSE	.42N .60W	0.5 0.5	+	-	U	6.0
20	34 09 117 31	47-5-20 21:17	3.1	P 59 R 22	TSN TSE TSN TSE	.49N .18W 1.18 1.6E	0.4 0.4 0.3 0.3	+	-	U	1.2 33
21	34 10 117 29	44-4-15 20:10	3.3	P 60	BLN BLE	1.0N .40E	0.6 0.6	+	+	D	1.2
22	34 10 117 29	44-4-22 22:10	3.0	P 60	TSN TSE	.20N .20E	0.4 0.4	+	+	D	3.2
23	34 10 117 36	48-10-2 19:34	2.7	P 51 R 28	TSN TSE TSN TSE	.11N .11W .88N .46E	0.5 0.5 0.3 0.3	+	-	U	0.3 1.4
24	34 11 117 32	48-2-5 12:44	3.5	P 57	TSN TSE	.25N .56W	0.5 0.5	+	-	U	13
25	34 11 117 32	48-2-5 12:44	3.5	R 25	TSN TSE	.70N .24E	0.3 0.3	-	-	U	1.7
26	34 11 117 35	48-10-2 18:46	4.0	P 52	TSN TSE	1.4N 1.5W	0.5 0.5	+	-	U	3.5
27	34 12 117 29	48-8-31 00:49	2.8	P 62 R 24	TSN TSE TSN TSE	.21N .18W .42N .35E	0.4 0.4 0.4 0.3	+	-	U	2.3 2.8
28	34 12 117 30	48-2-29 21:05	2.3	R 26	TSN TSE	.28N .28E	0.3 0.3	-	+	D	11
29	34 13 117 30	44-6-7 13:10	3.5	P 64	TSN TSE	.50N .50W	0.4 0.4	+	-	U	2.3
30	34 14 117 04	47-2-10 01:38	2.8	R 38	TSN TSE	.52N .23W	0.3 0.3	+	+	D	0.7
31	34 15 117 34	44-10-21 22:28	3.1	P 52	TSN TSE	.42N .35W	0.4 0.4	+	-	U	2.0

No.	Lat Long	Day Time	M.	Sta Dist	Inst	Ampl	Per	v	u	w	SV/SH
C											
32	34 15 117 35	44-12-21 18:20	3.1	P 49	TSN TSE	.53N .28W	0.4 0.4	+	-	U	0.8
33	34 16 117 09	48-12-10 17:54	3.0	R 33	TSN TSE	.88N .42E	0.4 0.3	+	+	D	15
34	34 16 117 14	48-7-25 21:39	3.0	P 88	TSN TSE	.11S .18E	0.5 0.4	-	+	D	5.0
35	34 16 117 14	48-7-25 21:39	3.0	R 32	TSN TSE	1.8S 2.5W	0.3 0.3	+	-	U	7.5
36	34 17 117 38	45-2-25 19:02	2.7	P 50	TSN TSE	.18N .28W	0.4 0.5	+	-	U	3.1
37	34 20 117 00	48-12-11 11:04	2.8	R 50	TSN TSE	.21N .53W	0.4 0.5	+	-	U	1.5
38	34 20 117 07	45-10-31 12:41	3.7	P 98	TSN TSE	.21N .35W	0.3 0.4	+	+	D	13
39	34 23 117 37	46-8-18 01:57	3.3	P 55	TSN TSE	.49N .80W	0.3 0.3	+	-	U	2.0
40	34 24 117 56	46-1-13 09:12	3.7	P 35	TSN TSE	4.9N 4.5W	0.4 0.4	+	+	D	0.7
B											
1	34 00 118 08	44-11-14 13:32	2.5	P 17	TSN TSE	.70S .35E	0.3 0.3	+	+	D	36
2	34 00 118	43-5-8 07:07	3	P 24	TSN TSE	2.7S 1.7W	0.4 0.3	-	+	D	4.0
3	34 00 118 16	49-9-18 21:08	3.1	P 18	TSN TSE	1.2S 1.2S	0.4 0.4	+	+	D	∞
4	34 00 118 22	47-7-9 23:16	2.8	P 20	TSN TSE	.32S .28W	0.4 0.5	+	+	D	160
5	34 00 118 22	47-7-9 23:16	2.8	R 87	TSN TSE	.21N ?	0.3 0.3	-	0	0	0
6	34 00 118 33	45-7-24 10:18	2.5	P 39	TSN TSE	.25S .18W	0.6 0.6	+	+	D	6.8

No.	Lat Long	Day Time	M.	Sta Dist	Inst	Ampl	Per	v	u	w	SV/SH
B											
7	34 00 118 43	42-10-9 11:16:35	3	P 53	BLN BLE	.50S .75E	0.6 0.6	+	-	U	3.4
8	34 01 118 02	43-12-7 06:46	2.5	P 30	TSN TSE	.21S .45E	0.4 0.5	+	-	U	0.8
9	34 02 118 00	43-6-12 13:11	2.5	P 22	TSN TSE	.50S .30E	0.3 0.3	-	+	D	11
10	34 02 118 18	46-6-29 21:22	2.4	P 18	TSN TSE	.35S .25E	0.5 0.4	+	-	U	0.5
11	34 03 118 03	48-12-1 07:20	2.4	P 14	TSN TSE	.70N .46W	0.3 0.4	+	+	D	9.0
12	34 03 118 05	46-2-20 05:11	2.8	P 13	TSN TSE	2.8N 2.4W	0.4 0.4	+	-	U	∞
13	34 05 118 07	49-2-22 07:39	2.8	P 17	TSN TSE	.35S .21E	0.3 0.3	+	-	U	4.0
14	34 06 118 33	46-9-7 13:10	2.5	P 37	TSN TSE	.25N .14W	0.4 0.4	+	+	D	0.7
15	34 08 118 14	48-1-19 05:35	1.3	P 7	TSN TSE	.10S .17W	0.5 0.5	+	-	U	2.5
16	34 11 118 10	48-8-2 17:55	2.1	P 5	TSN TSE	.46S .35W	0.4 0.4	+	+	D	2.2
17	34 11 118 10	48-8-2 18:05	2.0	P 5	TSN TSE	.52S .49W	0.4 0.4	+	+	D	0.8
18	34 11 118 10	48-8-2 18:08	1.9	P 5	TSN TSE	.28S .28W	0.4 0.4	+	+	D	0.5
19	34 15 118 40	48-6-17 10:49	2.8	P 47	TSN TSE	.18N .11W	0.5 0.5	-	+	D	3.5
20	34 19 118 53	45-12-20 02:17	2.3	P 19	TSN TSE	.35S .28E	0.4 0.4	-	-	U	23
21	34 23 118 50	48-5-13 00:52	2.5	P 65	TSN TSE	.18N .18W	0.3 0.4	-	+	D	13
22	34 24 118 34	43-4-20 00:43	3	P 44	TSN TSE	.63N .35E	0.4 0.4	-	-	U	0.9

No.	Lat Long	Day Time	M.	Sta Dist	Inst	Ampl	Per	v	u	w	SV/SH
B											
23	34 25 118 29	47-12-26 02:14	2.4	P 42	TSN TSE	.11N .21E	0.6 0.6	-	-	U	1.2
24	34 25 118 50	46-6-1 03:06	4.1	P 53	TSN TSE	.49N .70E	0.7 0.5	-	-	U	2.3
25	34 29 118 59	42-9-3 22:34	4.5	P 83	TSN TSE	2.3N 2.3E	0.5 0.5	-	-	U	1.2
26	34 29 118 59	42-9-3 06:06	4.5	P 83	TSN TSE	3.7N 1.4E	0.5 0.5	-	+	D	0.2
27	34 33 118 57	43-4-8 05:22	3	P 85	BLN BLE	.50N .75W	0.6 0.6	0	+	D	∞
28	34 34 118 40	43-7-18 10:30	2.5	P 137	TSN TSE	.30N .20E	0.3 0.3	-	+	D	0.9
29	34 38 118 25	43-3-12 00:00	3	P 60	TSN TSE	.21N .35E	0.3 0.3	-	+	D	0.5
30	34 38 118 35	43-5-1 07:00	3	P 65	TSN TSE	.35N .23W	0.3 0.3	+	+	D	19
31	34 38 118 51	46-6-26 05:18	3.4	P 84	TSN TSE	.52N .35E	0.6 0.6	-	+	D	0.4
32	34 48 118 58	46-1-17 04:21	3.4	P 102	TSN TSE	.24S .46W	0.6 0.5	+	+	D	2.0
33	34 54 118 57	45-7-24 16:08	3.4	P 110	TSN TSE	.35N .14E	.04 .05	-	+	D	2.1
A											
1	34 00 119 01	46-4-27 00:45	3.1	P 80	BSN BSE	.30N .15E	0.4 0.4	-	-	U	4.5
2	34 06 119 29	44-9-7 08:32	3.5	P 120	TSN TSE	.18N .18E	0.5 0.5	-	+	D	4.0
3	34 16 119 31	44-4-12 07:33	4.0	P 122	BLN BLE	1.0N 1.8E	0.6 0.6	-	-	U	5.1
4	34 22 119 07	48-6-7 20:02	3.1	P 91	TSN TSE	.11N .21E	0.4 0.4	-	-	U	4.0

No.	Lat Long	Day Time	M.	Sta Dist	Inst	Ampl	Per	v	u	w	SV/SH
A											
5	34 22 119 20	44-11-11 14:05	3.2	P 120	BSN BSE	.12N .33E	0.3 0.4	-	-	U	5.4
6	34 41 119 00	43-4-6 34:41	4	P 96	TSN TSE	.70N .60E	0.5 0.6	-	0	0	0
7	34 53 119 01	48-4-3 07:00	3.4	P 112	TSN TSE	1.1S 2.5W	0.5 0.5	+	-	U	2.2

THE RELATIONSHIP OF THE MODELO AND RIDGE ROUTE
FORMATIONS IN THE SOUTHERN RIDGE BASIN,
CALIFORNIA

Thesis by
Peter Dehlinger

MINOR THESIS
In Partial Fulfillment of the Requirements
For the Degree of
Doctor of Philosophy

California Institute of Technology
Pasadena, California

1950

ACKNOWLEDGMENTS

The writer wishes to express his sincere appreciation to Dr. R. H. Jahns of the California Institute of Technology, who suggested this problem and under whose guidance the work was done. Ideas contributed during the course of discussions with Dr. J. P. Euwalda of the California Institute of Technology, Dr. F. D. Bode of The Texas Company, and Mr. M. C. Israelsky of the United States Geological Survey, facilitated the investigations in many ways. Microfaunal analyses of numerous samples were made by The Texas Company, and helpful identifications of various megafossils were kindly contributed by Dr. J. W. Durham of the University of California.

ABSTRACT

The Modelo formation and the overlying Ridge Route formation, as exposed in the southern part of the Ridge Basin, are similar in general appearance and consist of alternating beds of sandstone and siltstone. The contact between the formations is neither a sharp break nor is it characterized by an interfingering of sedimentary units. The two units differ in general strike by as much as 35 degrees in the area studied, although the strike grades uniformly from that of one formation to that of the other. This difference in attitude is believed to be a depositional feature, rather than one resulting from structural disturbance.

The Modelo formation thins markedly in a northerly direction, and the Modelo sea appears to have transgressed the area from south to north during a part of upper Miocene time. Subsequently this sea retreated from the area, while non-marine Ridge Route beds appear to have been deposited concomitantly from a northerly direction. No appreciable time lapse is evidence between the periods of marine and non-marine deposition. The lowermost of the Ridge Route formation beds may be fluvial deposits, but the remainder of the formation appears to be of lacustrine origin. In post-Pliocene time the region was folded into the Ridge Basin. The folding evidently was related to displacements along the adjacent San Gabriel fault.

TABLE OF CONTENTS

	Page
Introduction	1
Stratigraphy	
General Statement	4
Modelo Formation	6
Ridge Route Formation	20
Stream Terraces and Alluvium	26
Structural and Depositional History	27
Geologic History	30
References	31

INTRODUCTION

The Ridge Basin, so named by Eaton (1929, fig. 5 and p. 750), is a northwesterly trending structural basin between the San Gabriel and San Andreas fault zones in the southeastern Coast Range province of California. The rocks in the basin consist of marine upper Miocene sediments and an overlying, considerably thicker series of non-marine deposits. The marine and non-marine beds are lithologically similar and appear to be conformable. During the present investigations, an attempt was made to determine the nature and sequence of events that affected these beds during upper Miocene and post-Miocene time.

The area studied is in the southern part of the Ridge Basin (Fig. 1) north of Castaic, a town on U. S. Highway 99 about 45 miles north of Los Angeles. A northwest trending strip of ground about nine miles long and three miles wide was mapped in detail. This strip is in parts of Ts. 5 and 6 N., Rs. 16 and 17 W., S.B.B. and M.L. Most of it lies within the Violin Canyon quadrangle, Los Angeles County, and small parts of it are in the adjacent Redrock Mountain and Whitaker Peak quadrangles.

Some of the first detailed mapping in the area under consideration was done by Clements, whose findings are presented in a Ph. D. thesis (Clements, 1932), and as a shorter published paper (Clements, 1937). Numerous references to earlier reconnaissance work done in the vicinity of the Ridge Basin are included in the thesis. Eaton

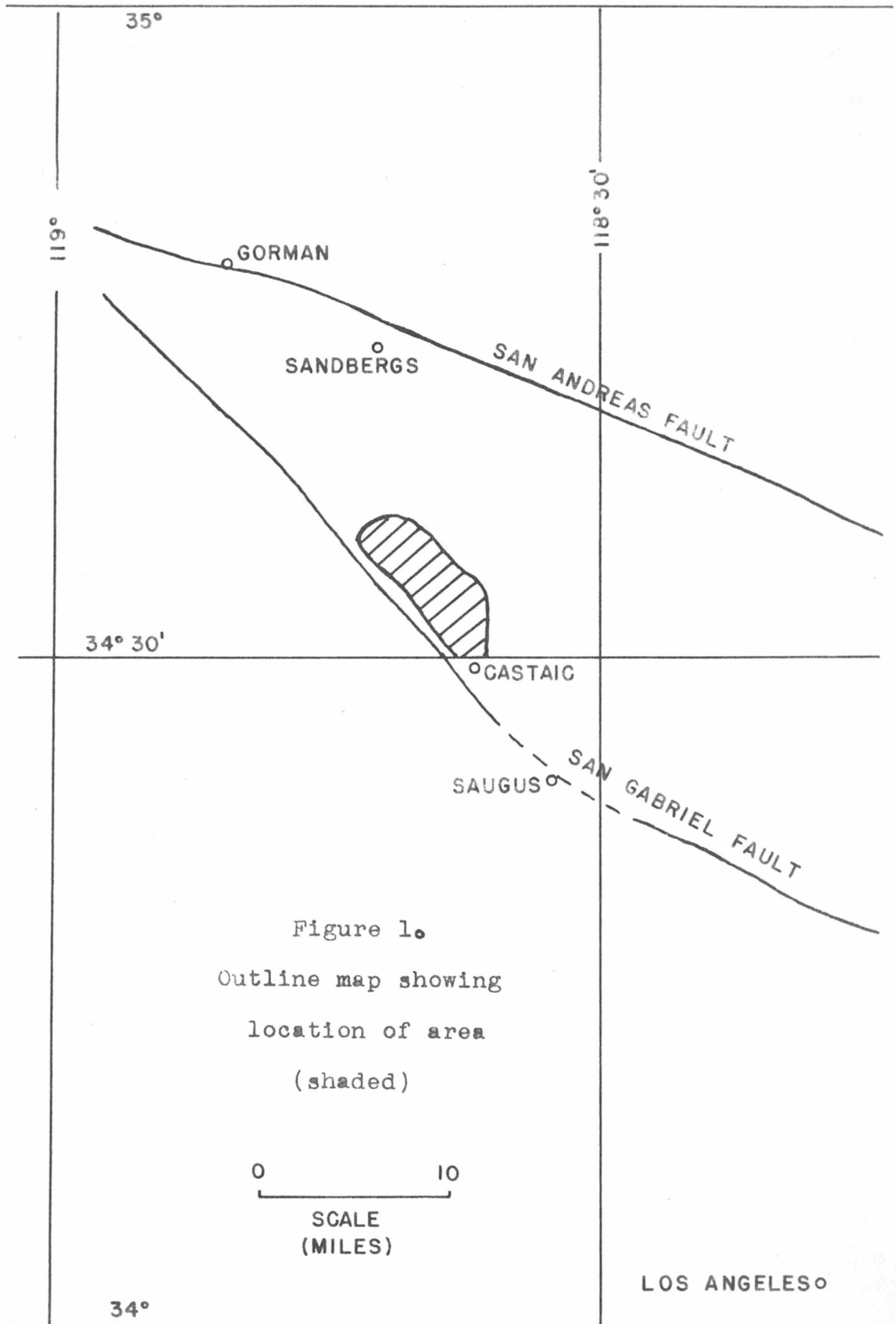


Figure 1.
Outline map showing
location of area
(shaded)

0 10
SCALE
(MILES)

LOS ANGELES

(1939) published the results of a reconnaissance study of the Ridge Basin. In 1947 students of a geological field camp of the California Institute of Technology mapped in detail the geology of the Red Mountain quadrangle, which adjoins the Violin Canyon quadrangle on the east. The results of this work have not yet been published. During the early 1930's a somewhat similar field camp was operated with headquarters at Sandbergs, a town approximately 10 miles north of the area discussed in this paper. Drs. J. P. Buwalda and F. D. Bode, directors of that camp, discussed their findings with the writer.

Field mapping in the present study was done on aerial photos (scale, 1" = 1666'). The field data were transferred from the photos to Los Angeles County topographic quadrangle sheets (scale, 1:24000).

STRATIGRAPHY

GENERAL STATEMENT

The two principal stratigraphic units in the southern part of the Ridge Basin are the Modelo formation (marine upper Miocene) and the Ridge Route formation (non-marine upper Miocene or Pliocene). Both these units consist primarily of alternating beds of sandstone and siltstone.

Igneous, metamorphic, and other sedimentary rocks are exposed beyond the area mapped. Most of these have been discussed by Clements (1932, 1937); those in the Red Mountain quadrangle, east of the area, have been mapped in detail by members of the 1947 geological field camp mentioned above. The following resume is largely abstracted from these two sources:

Metamorphic rocks

Two series of metamorphic rocks are exposed in the southern Ridge Basin. One, known as the Pelona schist, consists of coarse, granular, micaceous schists of probable pre-Cambrian age; the other comprises gneisses, quartzites, and marbles of possible Paleozoic age. The schists are exposed about five miles from the southeast border of the area, and the younger metamorphic rocks appear both east and west of the area. They crop out two or three miles to the east as well as about a mile to the west, where they are exposed on the west side of the San Gabriel fault.

Igneous rocks

Igneous rocks in the southern part of the basin consist of Jurassic (?) intrusive types, predominantly of granodioritic composition. These rocks are exposed over a considerable area, and the nearest outcrops are two to three miles northeast and northwest of the area investigated by the writer.

Sedimentary rocks

All sedimentary rocks in the southern Ridge Basin are of Cenozoic age. They comprise the following formations:

- Martinez (Lower Eocene)
- Domingine (Middle Eocene)
- Sespe (Oligocene)
- Vaqueros (Lower Miocene)
- Tambler (Middle Miocene)
- Mint Canyon (Upper Miocene)
- Modelo (Upper Miocene)
- Ridge Route (Upper Miocene or Pliocene)
- Pico (Pliocene)
- Saugus (Pleistocene)

Martinez and Sespe beds are exposed both east and west of the area. A narrow strip of the Mint Canyon formation is visible along the eastern boundary of the area, whence it extends several miles farther east. The Domingine, Vaqueros, and Tambler formations crop out a few miles west of the area. The Modelo formation is well exposed within the area, and extends beyond its north and west borders. To the west these beds are abruptly truncated by the San Gabriel fault, along which they are in contact with Pico beds and Paleozoic gneisses, quartzites, and marbles. The Modelo formation also is exposed one to two miles west of this fault.

The Ridge Route formation, also well exposed in the area, becomes thicker in a northwesterly direction, toward the deepest part of the Ridge Basin (Eaton, 1939). Pico and Saugus beds appear west and south of the area. Modelo beds overlie the Martinez formation with an angular unconformity east and northeast of the area. Southeast of the area Modelo beds overlie the Mint Canyon formation conformably in some places and unconformably in others.

MODELO FORMATION (UPPER MIOCENE)

The term "Modelo", as used in this paper, denotes marine beds of upper Miocene age. The term was defined by Eldridge (1907) to include beds that rest on the Vaqueros sandstone (which is younger than the Vaqueros formation) and that are overlain by the Fernando formation. Kew (1924) redefined the term to include the 2000 to 3000 feet of Vaqueros sandstone of Eldridge, so that the Modelo formation rests unconformably on the Topanga formation and is unconformably overlain by Pico beds. The Modelo formation has since been defined to include three divisions. The lower division is of Tumbler (middle Miocene) age, the middle believed to be of lower San Pablo (lower part of upper Miocene) age, and the upper of uppermost Miocene age (Hudson and Craig (1929). However, Kew's broader usage is followed in this paper.

Modelo beds crop out in approximately three-quarters of the area mapped. A conglomeratic member, ranging from a few to almost 300 feet



Plate I Exposure of basal Modelo conglomerates overlying the Martinez formation unconformably near the junction of Castaic and Fish Canyons.

in thickness, lies at the base of the formation (Clements, 1932). Boulders in this conglomerate consist of hard sandstones that are characteristic of the underlying Martinez formation, as well as quartzites, gneisses, and other rocks that represent the crystalline basement complex. A conglomeratic pecten reef, ranging from a few inches to about 8 feet in thickness and containing many fragments of pectens and oysters, overlies the basal conglomerates. This reef serves as an excellent marker unit. The thick Modelo section above the reef comprises alternating beds of sandstone, siltstone, and some shale.

The thickness of the Modelo formation changes markedly, but rather uniformly in a north-south direction. Approximately 6300 feet of the lower part of the formation is exposed in the southern part of the area, where upper Modelo beds have been removed by erosion. In contrast, the thickness of the entire formation in the northern part of the area is only 2000 feet. A reconnaissance examination north of the junction of Castaic and Fish Canyons indicates, however, that the Modelo beds do not pinch out or thin rapidly in areas farther north.

The Modelo beds have been folded into an asymmetrical, north-westerly plunging syncline, with a gentle northeast flank and a much steeper southwest flank. This fold is the southern part of the Ridge Basin, and is referred to by Clements (1932, 1937) as the Castaic syncline. U. S. Highway 99 extends along the axial part of this large fold. The San Gabriel fault (Palomas fault of Clements) is parallel to the synclinal axis, and lies about a mile west of it.

The rocks exposed along the eastern flank of the syncline form the chief basis for the discussions in this report.

The pecten reef that lies above the basal Modelo conglomerates is the oldest unit mapped in this study. The reef contains abundant fragments of Aequipecten raymondi and Ostrea titan. Other species of pectens also are reported from this horizon by Clements (1932). The rock is a coarse conglomeratic arkose with a calcareous cement; it is hard, well indurated, and has a limestone-like appearance. The unit is remarkably continuous, though it appears to pinch out locally.

The beds of Modelo sandstone, siltstone, and shale above the pecten reef are composed largely of subangular quartz fragments with varying proportions of biotite and feldspar. Biotite was observed in all these rocks, the largest quantities appearing in the siltstones and shales. Feldspar fragments are most abundant in the sandstones. The cement in the sandstones and siltstones appears to be calcareous and somewhat ferruginous. Numerous thin gypsum seams occur in many of the beds.

Thicknesses of the sandstone, siltstone, and shale beds commonly range from several inches to about five feet, though a few beds are as much as twenty feet thick. The sandstones range in texture from fine and sugary to coarse and less even. In some places they are pebbly, and even contain conglomeratic stringers. Most are buff to brown or drab, and a few show slightly reddish tinges. The colors of the siltstones are similar, but generally a little darker. The shales range from grey to dark bluish grey, and in some places they

have a bituminous appearance. Perhaps the most characteristic feature of the Modelo sandstone siltstone section is the rather monotonous sequence of beds that show alternations of texture but little variation in color or thickness.

Although many poorly preserved fossils occur at some horizons in the Modelo formation, most of the beds seem to be barren of such material. Foraminiferal remains are uncommon in even the unweathered parts of the darker shales. Several sandstone beds in the lower part of the formation, exposed in the southern half of the area, contain abundant casts and molds of mollusks. Such remains are rare in the upper beds of the formation, which do contain much fossil wood and charcoal. Several sandstone beds in the upper part of the formation contain penecontemporaneous deformations, indicating that slipping or "flowing" of beds occurred in the unconsolidated deposits.

Five stratigraphic columns of the part of the Modelo formation that lies above the pecten reef were made to show the nature of thinning of the formation (Fig. 2.). From these columns it appears that the formation, approximately 2000 feet thick in the northern part of the area, probably was more than 9000 feet thick prior to erosion in the southern part.

Column along line GG' (see pl. 4)

Basal Modello beds along line GG' lie east of the area studied. Both Clements and the 1947 California Institute of Technology field group show that the Modelo strata overlies the Mint Canyon formation in the region represented by this column. The thickness of the



Plate II Exposures of the Modelo sandstone and siltstone beds along the west hillside of Castaic Canyon.

section along this line is about 6350 feet. The section consists of alternating sandstone and siltstone beds; some parts of it contain relatively more sandstone, others relatively more siltstone.

From top to bottom, this section is as follows:

- - - -	
500'	Sandstone with interbedded siltstone and shale, forming the ridge along which the old Ridge Route highway was built.
- - - -	
650'	Siltstone with interbedded sandstone, forming a dip slope along line GG'.
- - - -	
1700'	Sandstone with interbedded siltstone and shale forming the abrupt ridge on the west side of Castaic Canyon.
- - - -	
1850'	Siltstone with interbedded sandstone and shale. Some of the sandstone members form small ridges. Most of this unit forms the gentle east slope of Castaic Canyon.
- - - -	
1650'	Alternating beds of sandstone and siltstone, with several sandstone beds forming hogback ridges.
- - - -	
	Base of Modelo formation.

Numerous megafossils but few foraminifera were found in the section covered by this column. Fragments of Protocardia centifolosa and casts and molds of Delectopecten and Spigula were identified.

Column along line CC'

Line CC', about a mile and a half northwest of line GG', traverses approximately 5400 feet of section. The section is not complete, as some upper Modelo beds have been removed by post-Miocene erosion. A brief description of the exposed section is as follows:

- - - -	
1250'	Sandstone beds separated by numerous siltstone layers.
600'	Siltstone with interbedded sandstone and shale. A few of the sandstone beds are ridge forming.
1700'	Sandstone with interbedded siltstone and shale. This unit forms the gentle east slope of Castaic Canyon
1700'	Siltstone with interbedded sandstone.
50'	Sandstone with interbedded siltstone.
- - - -	Pecten reef.

No foraminifera were found in this part of the area, and only a few beds appear to contain megafossils. The pecten reef is well exposed at the base of the section. Specimens of Haplophragmoides were identified in sandstone beds approximately 1800' stratigraphically above this reef. Casts and molds of Pecten, Anadara, Spigula, Cardium (?), Delectopecten, Solen, and Crenella (?), as well as plant fragments, were found near the top of the section.

Column along line BB'

Line BB', about a mile and a half northwest of line CC', traverses approximately 5150 feet of beds, and represents almost the entire Modelo section in this part of the area. A description of the rocks is as follows:

- - - -	
300'	Sandstone and siltstone, in alternating beds.
1050'	Sandstone with interbedded siltstone and shale.
500'	Siltstone with interbedded sandstone
- - - -	
2600'	Alternating beds of sandstone and siltstone, forming the escarpment between Castaic Canyon and the old Ridge Route highway.
700'	Siltstone with interbedded sandstone.
- - - -	Pecten reef.

No foraminifera and few casts and molds of megafossils were found in these rocks, which are more barren than those exposed along line CC'. Several Radiolaria and fish bones, found about 700' stratigraphically above the pecten reef were identified. Near the top of the section several casts of Delectopecten and Spigula were recognized.

Column along line AA''

Line AA'' is about a mile northwest of line BB'. The entire Modelo formation is exposed along this line, and consists of about 3500 feet of section above the pecten reef. The formation is overlain conformably by non-marine beds. A brief description of the Modelo section is as follows:

- - - - Top of Modelo formation
- 1600' Sandstone with interbedded siltstone and shale, forming the hogback ridge on which the old Ridge Route highway is located.
- - - -
- 1300' Sandstone, siltstone, and shale in alternating beds.
- - - -
- 100' Sandstone with interbedded siltstone and shale.
- - - -
- 500' Siltstone with interbedded sandstone.
- - - - Pecten reef.

Foraminifera, probably of Mohanian age, were found near the top of the formation in the vicinity of this line of section. They proved very helpful in locating the contact between the marine and the overlying non-marine beds. In general, however, few fossils were found in the section noted above.

Column along line EE'

Line EE', near the northern border of the area, is about a mile and a half northwest of line AA". The section traversed by this line is approximately 2000 feet thick, and is overlain conformably by a section of non-marine beds. The marine section includes the following units:

- - - - Top of Modelo formation.
- 850' Sandstone with interbedded siltstone.
- - - -
- 1150' Siltstone with interbedded sandstone and shale.
- - - - Pecten reef.

In general, the section along this line yields very little fossil material. A few casts of Spigula and Tritanalia (?) were found in one sandstone bed. The pecten reef is here characterized by a higher ratio of oyster to pecten remains than in other parts of the area. A few foraminifera were found near the base of the section, but these are thought to be of Eocene age. Presumably they represent reworked material derived from adjacent areas underlain by Martinez rocks.

The thinning of the Modelo formation in the southern Ridge Basin is illustrated in Figure 3, in which the five stratigraphic columns (Fig. 2) are drawn and spaced to the same vertical and horizontal scale. It is evident from the figure that in general the pecten reef is inclined 15 to 20 degrees more steeply than beds higher in the section. This difference in attitude appears to be a result of a

north to northeastward transgression of the sea, caused either by a uniform sinking of the region or by sinking and southerly tilting. The relations shown in Figure 3 suggest that: (1) the pecten reef was deposited on a rather uniform slope of about 15 degrees and the overlying sands and silts rapidly filled the basin as the sea transgressed; (2) the transgression probably was accompanied by a uniform sinking of the southern part of the area, south of line BB'; and (3) the northern part of the area (between lines BB' and EE') possibly may have been involved in a slight southerly tilt, as well as sinking, during transgression of the sea. The coarse arkosic character of the pecten reef may well suggest a steep slope of deposition, and the limited thickness of the reef suggests that favorable environmental conditions for its development were of comparatively short duration. Such depositional conditions would be in accord with the concept of a transgressing sea. That pecten and oyster reefs can form with such steep initial dips is evidenced by observations of modern reefs off parts of the coast of Baja California.*

The sinking of the southern part of the Ridge Basin appears to have ceased in upper Modelo time. Subsequent retreat of the Modelo sea was brought about either by a northerly tilting of the region or by a filling of the Modelo basin with sediment.

The Modelo fauna indicates deposition in upper Miocene time. Foraminiferal data further suggest deposition during Mohnian,

*Oral communication, Dr. F. D. Bode.

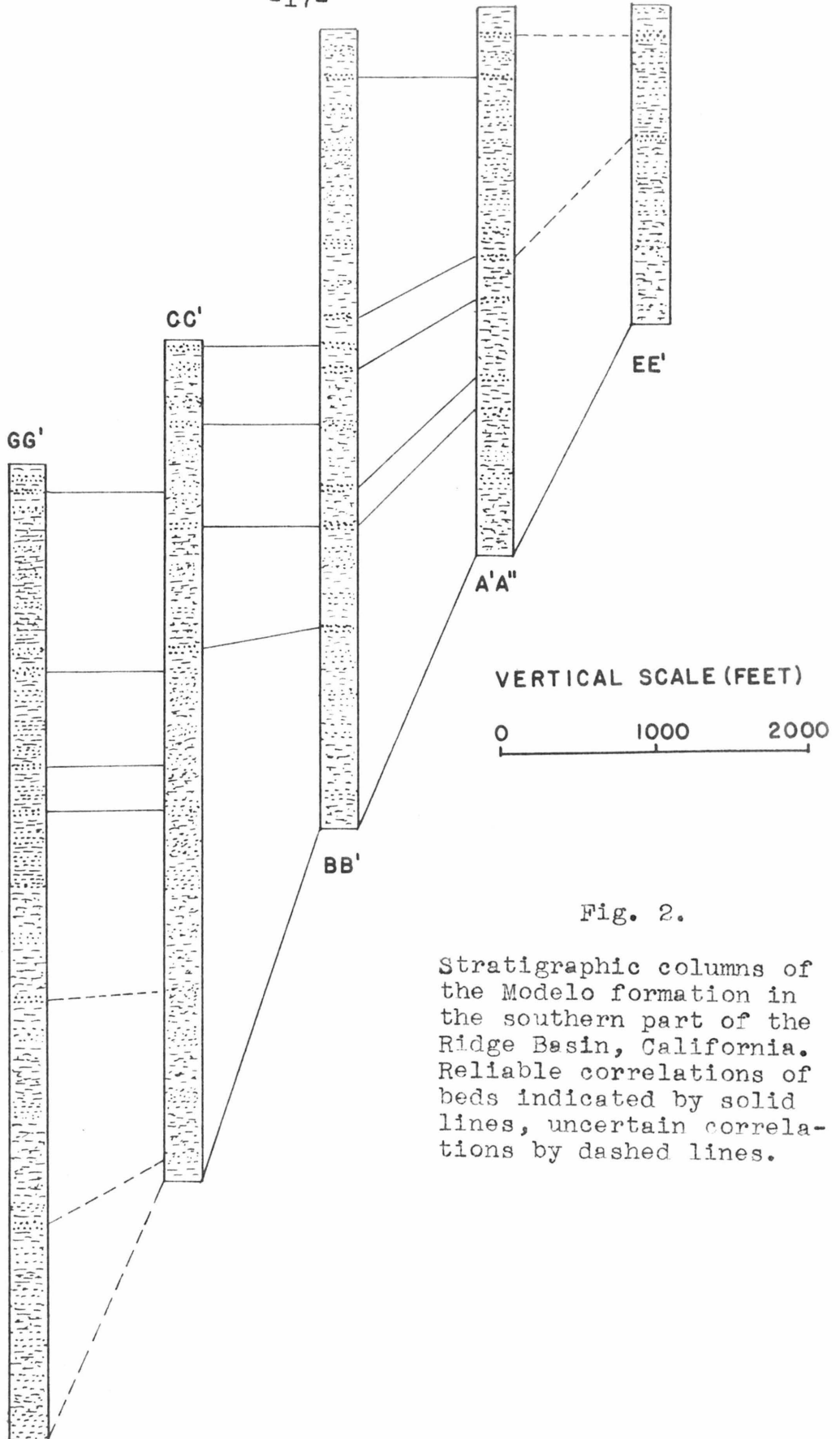


Fig. 2.

Stratigraphic columns of the Modelo formation in the southern part of the Ridge Basin, California. Reliable correlations of beds indicated by solid lines, uncertain correlations by dashed lines.

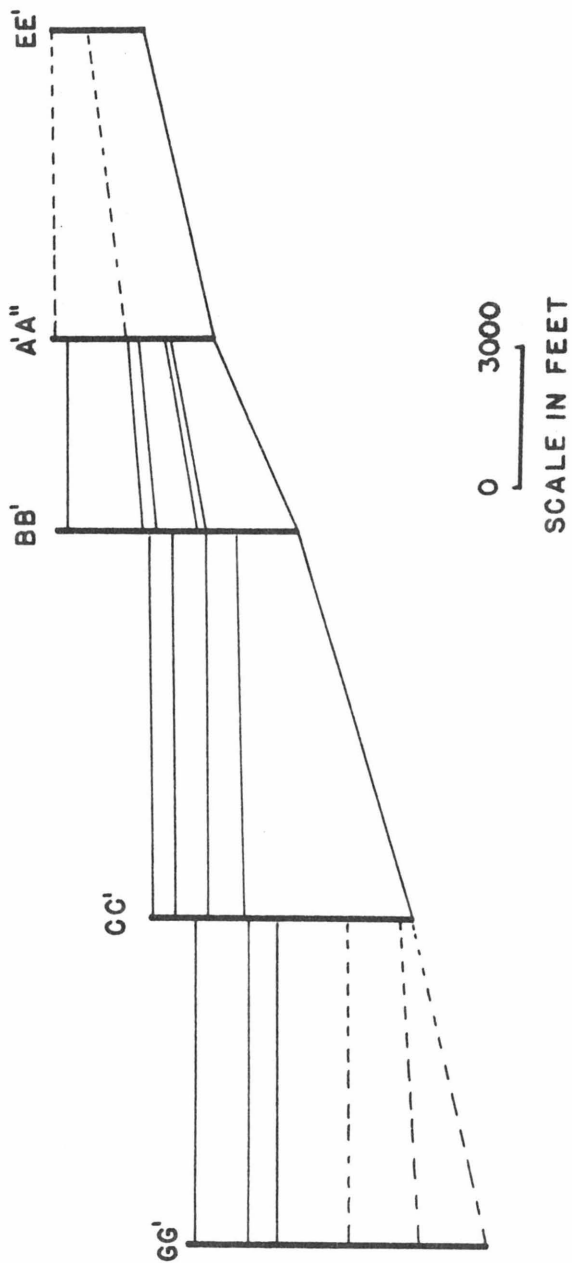


Fig. 3. Stratigraphic columns of the Modelo formation shown in figure 2, drawn to the same horizontal and vertical scales. Lowermost correlated horizon is the pecten reef.

but probably not during Delmontian time. Faunas identified from the Modele beds in this area include:

- Ostrea titan Conrad
- Aequipecten raymondi Clark ?
- Protocardia centifilosum (Carpenter)
- Pecten sp.
- Delectopecten sp.
- Spigula sp.
- Solen sp.
- Andara sp.
- Crenella sp.
- Cardium sp.
- Radiolaria sp.
- Haplophragmoides sp.
- Diatoms
- Foraminifera (probably Mohnian)
- Fish bones

RIDGE ROUTE FORMATION (UPPER MIOCENE OR PLIOCENE)

The Ridge Route formation is a thick series of non-marine beds that overlie the Modelo strata in the Ridge Basin. The term "Ridge Route" was introduced by Clements (1937).^{*} The formation has been described in a general way by Eaton (1939), who believed that it has a thickness of about 18,000 feet in the central part of the Ridge Basin.

The lowermost 5100 feet of the formation appears in the area of the present study. It contains some fresh-water and brackish-water ostracods and a few fish bones, but otherwise appears to be devoid of fossils. The age of the formation cannot be determined precisely on paleontologic grounds. However, it rests conformably on Modelo beds of probable Mohnian age, so that the lowermost of the continental beds may well be Dehmontian in age. These beds might thus be classed as latest upper Miocene or early Pliocene.

The Ridge Route formation crops out in the northwestern part of the area, and extends over approximately one quarter of the area that was mapped. The rocks resemble the underlying marine strata in lithology and general appearance. The contact between the formations is gradational, and is difficult to locate in the field. Although the two units are not readily differentiable by inspection, some

^{*}Dr. J. P. Buwalda previously had applied the name to continental beds mapped by members of the California Institute geological field camp located at Sandbergs, but had not placed it in the published record.

lithologic features help to distinguish them. The non-marine sandstones generally are sandier, coarser, and constitute a larger part of the section than the Modelo sandstone beds. They also contain many more lenses and stringers of pebbly conglomerate, and are more continuous, more massive, are thicker, and have greater resistance to erosion. The topography developed on the continental beds is more rugged and includes hogback ridges of greater relief than that developed on the Modelo beds. As a result, the non-marine sandstone beds can be traced more distinctly and reliably on aerial photographs than the marine beds.

Shale beds are rare in the non-marine series exposed in this area, but siltstone layers, many of them thinly bedded, are common. Most of the formation in the southern Ridge Basin has been weathered considerably, and has a more friable appearance than either the fresher parts of this formation or the underlying marine beds.

The color of the Ridge Route sandstone reefs is similar to that of the Modelo sandstones, ranging from buff to tan, brown, and drab. The non-marine siltstone beds are generally a little darker than the sandstones. Gypsum veins, observed in many of the Modelo beds, are rather rare in the lower part of the continental series. Like the Modelo strata, the Ridge Route beds consist primarily of sub-angular quartz fragments, with numerous biotite flakes and feldspar particles. In contrast to those in the Modelo sandstones, the average quartz fragment of the Ridge Route sandstones appears larger, and the biotite flakes are more abundant. The angularity of the fragments

in the two formations is similar. The two units appear to have been derived from similar sources, or possibly even the same source.

The Ridge Route beds have been folded concordantly with the underlying Modelo strata into the northwesterly plunging Castaic syncline. Although the east limb of the fold was the primary object of this study, the non-marine strata are so markedly different on the two flanks of the fold that a brief lithologic description of the west flank seems desirable.

About 1000 to 2000 feet west of the synclinal axis, in the vicinity of Canton Canyon, sandstone and siltstone beds typical of the east flank of the fold pass abruptly along the strike of the formation into a thick, steeply dipping series of massive, poorly bedded conglomerates. Clements (1932, 1937) indicates that these beds extend westward, with a steep dip, to the San Gabriel fault. The boulders in the conglomerates are subangular, ranging in size from a few inches to about three feet. They consist of granitic, dioritic, and gneissic rocks, which probably were derived from highlands that existed west of the fault during much of Ridge Route time. No extensive conglomerated beds are present east of the synclinal axis, although rather thin conglomerate lenses occur with the sandstones. Pebbles in these conglomerates, generally less than three inches in diameter, are fairly well rounded and consist of sandstone, quartzite, and some granitic rocks. These clasts probably were derived from the highlands north and east of the area, as they are similar to those found in the Martinez beds.

Near the base of the non-marine section, along the old Ridge Route highway, mud cracks and thin layers and seams of silt evidently formed in the drying-up stages of a water-laid deposit can be seen. In its initial stages of deposition, the Ridge Route formation apparently was covered by water only intermittently, and may have been of fluvial origin. A short distance above the base of the formation a lacustrine origin is suggested by the presence of ostracods, probably of fresh water affinities, as well as by the general continuity and lithology of the beds. Both Clements (1932, 1937) and Eaton (1939) have interpreted the formation as a lacustrine deposit.

Thicknesses of individual sandstone layers in the non-marine section generally range from a few inches to about 20 feet, with some of the largest sandstone reefs more than 50 feet thick. The beds appear to be continuous and remarkably constant in thickness within the area studied. The formation thickens in a northerly direction as a result of overlapping beds. This suggests either a uniform sinking of this part of the basin during Ridge Route time, or a gradual rising of the lake level. Nowhere in the field was either a sharp contact or an interfingering of beds between the marine and non-marine formations observed. A gradational zone between the marine and lacustrine beds, consisting of brackish water and possibly fluvial deposits, does appear to exist. This zone, however, could not be completely isolated in the field, owing to lack of sufficient exposures. It is estimated that the thickness of beds between the marine and lacustrine parts of the section is of the order of 50 feet or less.



Plate III Exposures of the Ridge Route sandstone and siltstone beds along the west hillside of Castaic Canyon.

A columnar description of the Ridge Route formation, as exposed in the area of study, indicates a thickness of about 5050 feet as follows:

1000'	Sandstone reefs separated by siltstone beds.
400'	Siltstone with interbedded sandstone
1250'	Sandstone reefs with interbedded siltstone, forming the west hillside of Big Oak Flat Canyon.
1150'	Siltstone interbedded with sandstone, several beds of which form reefs. The series forms the approximate dip slope on the east side of Big Oak Flat Canyon.
550'	Sandstone reefs with interbedded siltstone.
150'	Siltstone with interbedded sandstone
500'	Thick pebbly sandstone reefs, containing numerous siltstone beds.
50'	Gradational zone between marine and lacustrine beds, containing many conglomeratic lenses.

Stratigraphic units higher in the Ridge Route formation can be traversed north of the area, particularly along the old Ridge Route highway and along U. S. Highway 99.

STREAM TERRACES AND ALLUVIUM (QUATERNARY)

Stream-terrace deposits cap many of the ridges in the vicinity of Castaic Canyon. These deposits consist of unconsolidated and poorly bedded gravels that vary in composition from place to place. They are subhorizontal, and range in thickness from a few inches to 150 feet or more. The thickest terrace deposit in the area is exposed at the junction of Castaic and Elizabeth Lake Canyons. The levels of preserved remnants of terraces range so greatly that correlations are difficult to make, but the deposits indicate that the Castaic stream once flowed at levels felt higher than the present floor of the southern part of the canyon. Many stages in the downward cutting of the stream are indicated.

Alluvial deposits form the floors of all the larger canyons and extend well toward the heads of the smaller ones. About 80 feet of alluvium was logged in a well drilled in Castaic Valley, in the southeastern part of the area. The thickness of the alluvial deposits is apparently not great in most places, however.

STRUCTURAL AND DEPOSITIONAL HISTORY

The dominant structural feature in the area is the asymmetrical northwest plunging southern part of the Ridge Basin, commonly referred to as the Castaic syncline. This fold is parallel to the San Gabriel fault, and its axis lies about a mile east of the fault. The steep limb of the fold lies west of the axis, where beds are locally overturned. The east flank dips rather uniformly at about 20 degrees, and numerous resistant beds form hogback ridges.

A minor anticlinal fold is parallel to the Castaic syncline in the vicinity of upper Canton Canyon. Its axis lies about 1000 feet southwest of the main synclinal axis. The anticline extends beyond the boundary of the area, and appears to be several miles long. Numerous small folds are present in the vicinity of the main synclinal axis; some of these are recumbent. Many of the folds are exposed along U. S. Highway 99.

A northwest-trending anticline lies in the southeastern part of the area, and extends southeastward into the area of the adjoining Red Mountain quadrangle. The fold is in sec. 13, T. 5 N., R. 17 W., and in secs. 18 and 19, T. 5N., R. 16 W. Members of the 1947 California Institute geological field camp have shown it to extend southeastward toward Charlie Canyon. This flexure has been drilled for oil on several occasions, the first in the late 1890's. The maximum depth reached by one of these wells was 3404 feet. The hole was bottomed in Modelo beds. Several of the wells encountered showings of gas at different horizons.

An anticlinal fold appears to exist just to the southeast of the area mapped. It has been drilled recently to a depth of 2800 feet. Some oil production was reported near the base of the Modelo formation or the top of the underlying Mint Canyon formation at a depth of about 2300 feet.

No major faults lie within the area of present investigation, and only a few minor breaks were observed. These smaller faults have displacements of 15 feet or less, and hence are not shown on the map. Directions of displacement are generally not determinable; several of the faults, however, may be of a strike slip type, with the same movement sense as that along the San Andreas fault zone.

The Modelo sea invaded the southern Ridge Basin from a southwesterly direction, so that initial dips of the Modelo beds were in that direction. The marine transgression presumably was due to a sinking of the region, with possibly a slight southerly tilt over part of the area. In late Modelo time the sinking (and possible tilting) ceased, and appears to have been superseded by a north or northwesterly tilt of the region. The tiltings were very likely related to displacements along the San Gabriel fault. As the Modelo sea receded from the area, streams probably from a northerly direction evidently spilled their deposits over the Modelo sediments. The drainage probably was soon dammed by a northerly tilting of the area and a large lake was formed in and northwest of the area studied. The presence of Pliocene marine formations south of the Ridge Route beds, in the vicinity of Castaic, suggests that the dam was probably

not high. The lacustrine deposits apparently had northwesterly initial dips, which probably accounts for the difference in strike observed between these and the underlying marine beds. Source rocks for the marine and non-marine formations probably were similar, if not the same. The marine beds appear to have been derived from highlands east and north of the area, whereas the non-marine sediments appear to have been derived from highlands to the east and west.

The Castaic syncline appears to have been folded in post-Ridge Route time. Eaton (1939) states that the entire Ridge Route formation was folded into the Ridge Basin, dating the folding as probably post-Pliocene. The minor folds in the southern part of the basin probably were formed contemporaneously with the Castaic syncline. Folding in the Ridge Basin is very likely associated with movements along the San Gabriel fault.

Terrace deposits at different stream levels, in some places of considerable thickness, indicate that during Quaternary time streams in the area intermittently cut and filled their channels. Either variations in stream base level or a rising and lowering of the region is thus evidenced during part of the Quaternary period.

GEOLOGIC HISTORY

The following is the apparent chronological order of events in the southern part of the Ridge Basin since middle Miocene time:

1. The Modelo sea invaded the area from the south during upper Miocene time. This sea transgressed a land surface underlain by Martinez and Mint Canyon beds, and extended to points at least several miles north of the area studied. During much of Modelo time the region was sinking, with possibly some tilting toward the southwest.
2. A gradual tilting of the region in a north to northwesterly direction during late upper Miocene, probably Mohmian time, resulted in a filling of the Modelo sea with silt.
3. Streams from a northerly source spilled their deposits on the Modelo sediments, evidently with no appreciable time lapse between the two periods of deposition. These streams apparently were dammed to the south, thus forming a lake with its main body lying to the north, near the center of the Ridge Basin. This lake may have been formed during Delmontian or Pliocene time.
4. The Ridge Basin was formed by folding, probably reflecting movement along the San Gabriel fault during late Pliocene or Pleistocene time.
5. Minor intermittent changes in base level or elevation of the area occurred during Quaternary time, and resulted in cutting of numerous stream terraces and deposition of terrace gravels.

REFERENCES

Clements, Thomas.

1932. "The geology of the southeastern portion of the Tejon quadrangle, California," Ph. D. Thesis at the California Institute of Technology Library.

1937. "Structure of the southeastern part of the Tejon quadrangle, California," Bull. Am. Assoc. Pet. Geol., vol. 21, no. 1, pp. 212-232.

Eaton, J. E.

1929. "The by-passing and discontinuous deposition of sedimentary materials," Bull. Am. Assoc. Pet. Geol., vol. 13, no. 7, pp. 713-761.

1939. "Ridge Basin, California", Bull. Am. Assoc. Pet. Geol., vol. 23, no. 4, pp. 517-558.

Eldridge, G. H. and R. Arnold.

1907. "The Santa Clara Valley, Puente Hills, and Los Angeles oil districts, southern California", U.S.G.S. Bull. 309.

Hudson, F. S. and E. K. Craig.

1929. "Geologic age of the Modelo formation, California", Bull. Am. Assoc. Pet. Geol., vol. 13, no. 5, pp. 509-518.

Kew, W. S. W.

1924. "Geology and oil resources of a part of Los Angeles and Ventura Counties, California, U.S.G.S. Bull. 753.